G. Merisio, F. Topputo
Present-Day Model of Lunar Meteoroids and Their Impact Flashes for LUMIO Mission
Icarus, 2022, 115180 (22 pages)
doi:10.1016/j.icarus.2022.115180

Present-day model of lunar meteoroids and their impact flashes for LUMIO mission

Gianmario Merisio*[1] and Francesco Topputo†[1]

[1] *Department of Aerospace Science and Technology, Politecnico di Milano, Via La Masa 34, 20156, Milano, Italy*

Keywords: *Meteoroids*, *Impact flashes*, *LUMIO*, *CubeSat*, *Moon*.

Abstract

The Lunar Meteoroid Impacts Observer (LUMIO) is a CubeSat mission to observe, quantify, and characterize the meteoroid impacts by detecting their flashes on the lunar farside. It complements lunar nearside observations performed by ground-based observatories to yield global information synthesis on the lunar meteoroid environment. Predicting LUMIO's scientific outcome involves devising a methodology to model the meteoroid environment. We propose a method where numerous known meteoroid streams, as well as sporadic collisions with the lunar surface, are modeled. Impacts are generated with a stochastic approach based on experimental observations of fireballs, impact flashes, and meteors. A catalog collecting data of both meteoroid streams and sporadic background is made available to the community. Sample scenarios are reproduced to show the capabilities of our method. A synthesis of the statistical analysis performed on the collision dynamics is presented. Results show that a typical scenario counts almost 2 million impacts with impact kinetic energy larger than 10^{-7} kton TNT Equivalent, out of which approximately 200.000 fall in the energy range of interest for the LUMIO mission. For that subset, the equivalent black body temperature is estimated to range in $1510 - 2290\,\mathrm{K}$, the average impact flash duration is expected to be approximately $15\,\mathrm{ms}$, and the average plume area is predicted to be roughly $70\,\mathrm{m}^2$.

1 Introduction

Vast amounts of meteoroids and micrometeoroids continuously enter the Earth–Moon system and thus become a potential threat to future human and robotic

*PhD Student, gianmario.merisio@polimi.it (corresponding author)
†Full professor, francesco.topputo@polimi.it

assets that will inhabit the Moon for significant periods of time. This phenomenon has caused a substantial change in the lunar surface [1], the Moon having no protective atmosphere. Recent observations from NASA's Lunar Reconnaissance Orbiter (LRO) have provided direct evidence for the devastating effect of such collisions [2]. The impact rate on the lunar surface has important implications for future outposts that plan to inhabit the Moon for significant periods. Consequently, a greater understanding of the meteoroids population in the cislunar environment is required.

Meteoroids are small Sun orbiting fragments of asteroids and comets, whose sizes range from roughly 30 micrometers to roughly 1 meter [3, 4]. Their formation is a consequence of asteroids colliding with each other or with other bodies, comets releasing dust particles, and minor bodies shattering into individual fragments. Therefore, insight into meteoroids can be valuable for the study of asteroids and comets themselves. Since their orbits take between 10^3 to 10^5 years to randomize, many meteoroids still have orbits similar to their parent asteroid or comet, making it theoretically possible to associate them with the parent body [1]. Due to their size, meteoroids can only be detected when the Earth–Moon system crosses their orbit. Most annual streams are wider than the Earth–Moon distance, however sudden short-lived bursts of meteor activity called outburst may not. In the former case, an increase of meteoroid activity both in the Earth atmosphere and on the lunar surface is detected, giving rise to meteor showers or meteoroid impacts, respectively. Differently, meteoroids are classified as sporadic when belonging to the (almost) homogeneous background [3].

The parent body of a meteoroid can be identified according to the number of detected collisions in a given time frame, using the models of already known showers and sporadic sources [5, 6]. Therefore, since meteoroids are hardly observable directly, studying their impacts helps understanding the spatial distribution of near-Earth objects (NEOs) in the solar system. Furthermore, recorded collisions are used to refine the current meteoroid distribution models. Thus, a reliable meteoroid impact flux model is key for a risk assessment exercise, in view of the sustainable deployment of space assets. A better comprehension of the spatial distribution of meteoroid impacts across the lunar surface is needed. In particular, full-disk observations are necessary to explain asymmetries in the spatial distribution [1].

Using the Moon as a detector of meteoroids is also instrumental to predict collisions with the Earth. It is instrumental because studying the meteoroid flux at the Moon can be useful to understand the meteoroid flux impacting the Earth. Additionally, monitoring the Moon allows covering a much larger area than traditional methods monitoring Earth atmosphere. Furthermore, statistical data acquired by monitoring the Moon can be directly compared with the meteoroid data known so far and can fill the knowledge gap in the meteoroid population. The Tunguska event in 1908

is estimated to have released at least 10 megatons of TNT; an event that may occur in 1,000 years [7]. The smaller airburst of Chelyabinsk in 2013 produced a number of casualties [8]. All in all, refining current meteoroid models is of paramount importance for many applications.

LUMIO is a CubeSat mission that shall observe, quantify, and characterize meteoroid impacts on the lunar farside by detecting their flashes, so complementing ground-based observations on the lunar nearside [6, 9–16], to provide global information on the lunar meteoroid environment and contribute to lunar situational awareness [17]. LUMIO was awarded winner of European Space Agency (ESA)'s competition "Lunar CubeSat for Exploration", and as such it is being considered for implementation[1]. The Phase 0 study was carried out in 2017; an independent mission assessment by ESA followed in 2018; the Phase A study has been carried out in 2020–2021 under ESA's General Support Technology Programme (GSTP). The mission utilizes a 12U XL form-factor CubeSat which carries an optical instrument (LUMIO-Cam) capable of detecting light flashes in the visible spectrum [18, 19]. The mission implements a novel orbit design [20] and the latest CubeSat technologies to serve as a pioneer in demonstrating how CubeSats can become a viable tool for deep space science and exploration [21–24]. The operative Earth–Moon L_2 quasi-halo orbit of LUMIO is shown in Figure 1 [20].

In this paper, we present a stochastic model of the lunar meteoroid environment that was used to infer the scientific requirements of LUMIO. The model is based on experimental observations of fireballs, impact flashes, and meteors. These are collected in the form of a catalog mapping data of both meteoroid streams and sporadic background [12–14, 25–30]. The model we propose can be used to perform quantitative analyses to predict the likelihood of collisions on the lunar surface in a given time frame. It unifies methods [1, 20, 31], experimental observations [6, 32–35], and empirical laws [16, 36–38], which individually describe parts of the meteoroid impact phenomenon under a unique umbrella. In this regard, the model presented in this work is inherently different from similar methodologies. For instance, MIDAS [39] was developed to support flash detection, while performing systematic monitoring of the night side of the Moon from Earth using small telescopes. Although possessing similar functionalities, our model is intended to predict collisions before they occur. The envisaged methodology and reported catalog establish a procedural generation for meteoroid impacts that may prove useful for the relevant scientific community. We reproduced sample scenarios that fit the case of LUMIO to show the capabilities of the methodology. Throughout the paper, the model is also referred to as Meteoroid Gun (MeGun).

The remainder of the paper is organized as follows. In Section 2, the meteoroid envi-

[1] https://www.esa.int/Enabling_Support/Space_Engineering_Technology/CubeSats_for_hunting_secrets_in_lunar_darkness [last accessed 01/12/2021].

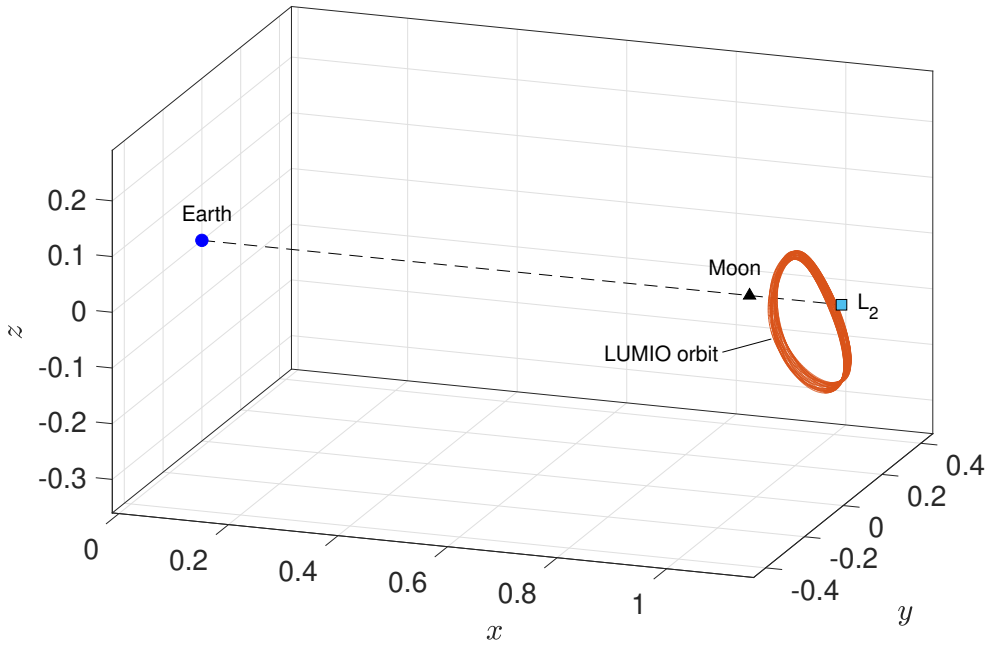

Figure 1: Operative Earth–Moon L_2 quasi-halo orbit in the Earth–Moon rotating frame in dimensionless coordinates (length unit equal to Earth–Moon distance).

ronment modeling is introduced. Details on the generation of meteoroid streams and sporadic background impacts are discussed in Section 3 and 4, respectively. A summary of the generation procedure follows in Section 5. Then, results of the simulated scenarios are shown in Section 6. Concluding remarks are given in Section 7.

2 Modeling of the meteoroid environment

In the MeGun model, each meteoroid is generated individually. The generation is based on experimental observations of fireballs, impact flashes, and meteors performed in recent years. The inputs are the desired target (the Moon in this case), the time span to be covered, the time step, and the minimum kinetic energy of meteoroids to generate. The latter is needed because meteoroid population is unbounded for decreasing kinetic energy, hence, a lower bound has to be set to reproduce a finite number of objects. The model embeds the Spacecraft Planet Instrument Camera–matrix Events (SPICE) toolbox to carry out a number of tasks ranging from pure reference frame conversion to more refined geometric transformations [40, 41].

The meteoroid environment is made up of two main components: the meteoroid streams, and the sporadic background. Meteoroids belonging to those categories are generated with different procedures. The two sets are then merged together. At the

end, all meteoroids are characterized by the same set of descriptors (see Section 3).

2.1 Meteoroid streams

The international astronomical union (IAU) keeps track of reported meteor showers[1]. Showers are reported to IAU and added to the Meteoroid Data Center (MDC) database[2]. To date, there are 932 reported showers in the database. Among them, 112 are established showers [42, 43]. The catalog contains the data of all established showers. Nonetheless, the complete set of data is not available for all showers. The lack of important parameters in the literature is an indicator of insufficient observations. In general, this happens when a shower is characterized by a small flux of meteoroids, which translates in a low zenith hourly rate ZHR. In that case, the shower flux is considered negligible and the shower is discarded. Consequently, only a subset of the established showers is used to generate the corresponding meteoroid streams (see Appendix A, Table 6).

To build up a comprehensive catalog, information available in the literature [12–14, 25–29] have been harmonised; see Table 7 in Appendix A. Yearly variations in the flux and in the epoch (solar longitude) of activity peak, and rare events like outbursts are not considered. Therefore, information about those phenomena is not provided in the catalog.

2.2 Sporadic background

The sporadic background is modeled taking into account 6 different sources: helion source (HE), anti helion source (AH), north apex source (NA), south apex source (SA), north toroidal source (NT), and south toroidal source (ST). To each source is associated a radiant expressed in terms of ecliptic longitude λ and latitude β, a velocity distribution, and a relative strength S (see Appendix A, Table 8) [30, 44–47]. Velocity distribution of the whole sporadic background also exists in the literature [45–48]. In the radiant-resolved model proposed in [30], an additional isotropic source (ISO) is modeled. However, recent works avoid modeling the ISO since the sporadic complex seems not isotropic in its directionality [45, 47, 49].

The parameter describing the sporadic background flux is the hourly rate HR. In literature, the common practice is to use $\mathrm{HR} = 10\,\mathrm{h}^{-1}$ [6, 16, 39]. The dependence of the hourly rate HR on the average zenithal radiant distance can be assumed weak because sporadic meteoroids radiate from very diffuse areas [50].

[1] Information about a meteoroid stream is obtained from the corresponding meteor shower.
[2] https://www.ta3.sk/IAUC22DB/MDC2007 [last accessed 01/12/2021].

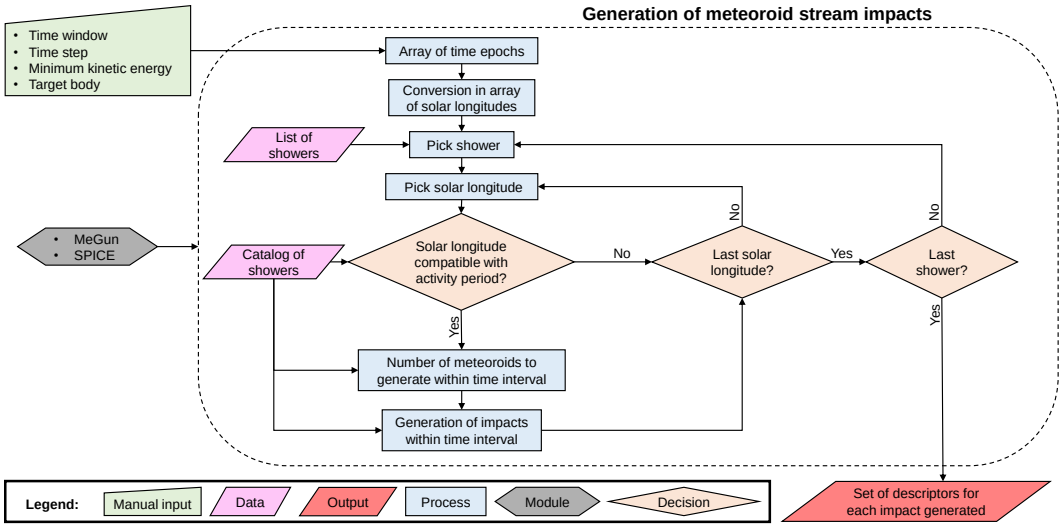

Figure 2: Schematic representation of the generation procedure for meteoroid stream impacts.

3 Modeling of meteoroid streams

The generation procedure is key in our model. The process is identical for each stream, and it is performed recursively for all streams modeled. At the end, each meteoroid impact generated is characterized by a set of descriptors, which are described in details in the remainder of this Section. Figure 2 shows a schematic representation of the procedure.

3.1 Initialization

Showers parameters are time dependent, thus, knowledge of the epoch is needed throughout the simulation. The model takes as input the time window to simulate and the sampling time. The vector of time epochs $\{t_0, t_1, \ldots, t_i, \ldots, t_N\}$ is built with the time step Δt. In essence, meteoroids are generated within small time intervals of amplitude Δt centered around the time epochs t_i. Then, the array of time instants is converted in an array of solar longitudes.

With reference to Figure 2, the first shower from the list of those considered (see Table 6 in Appendix A) is selected. Impacts belonging to the meteoroid stream are generated on time epochs and solar longitudes overlapping with the activity period of the shower. Information about the shower is retrieved from the catalog in Appendix A (see Table 7). The procedure is repeated for every shower in the list. Each impact has a set of descriptors that are detailed in the following subsections.

3.2 Number of meteoroids

The number of meteoroids $\mathcal{N}$ impacting the Earth with kinetic energy higher than a threshold $\mathrm{KE_{min}}$ is computed in the metre, kilogram, and second system of units (MKS) as [51]

$$\mathcal{N}_{\oplus} = \int_{t_i - \frac{\Delta t}{2}}^{t_i + \frac{\Delta t}{2}} N_{6.5} \left(\frac{2\mathrm{KE_{min}}}{V_{\mathrm{imp},\oplus}^2 m_{6.5}} \right)^{1-s} \mathrm{d}t \tag{1}$$

where $N_{6.5}$ is the number of meteoroids impacting the Earth with absolute magnitude +6.5 or brighter per unit time; s is the mass distribution index; $V_{\mathrm{imp},\oplus}$ is the average impact velocity at Earth of the shower, computed correcting the geocentric velocity for the gravitational acceleration. Equation (1) is applied individually to each meteor shower. The geocentric velocities of all meteor showers are summed up in Table 7, which reports data available in the literature. $m_{6.5}$ is the mass of a meteoroid corresponding to a meteor of absolute magnitude +6.5 at the Earth. The absolute magnitude M is conventionally computed at 100 km altitude for meteors [28]. Equation (1) treats showers using the mass distribution index. This is to get the number of impacts to generate in a given time period and range of kinetic energy. The mass distribution index s is linked to the population index χ through the relation

$$s = 1 + 2.5 \log_{10}(\chi). \tag{2}$$

The population index of a shower is derived experimentally. It express the ratio between the number of meteoroids with magnitude $(M + 1)$ and the number of meteoroids with magnitude M [52].

To get $m_{6.5}$ for a specific shower the following relation is used [53]

$$m = 10^{-3} \left(\frac{10^{\frac{40-M}{2.5}}}{7.7 \times 10^{-10} (10^5 V)^{3.91}} \right)^{\frac{1}{0.92}} \tag{3}$$

where m is in kg, M is the absolute magnitude, and V is the shower geocentric velocity in $\mathrm{km\,s^{-1}}$. The value $M = +6.5$ is used to get $m_{6.5}$. Equation (3) has been obtained inverting Equations (1) and (2) in [53].

$N_{6.5}$ can be expressed as a function of the zenith hourly rate ZHR following [28, 52–54]. To model the time dependence of the ZHR the following relation is used [29]

$$\mathrm{ZHR} = \mathrm{ZHR}^{\max} \frac{(W/2)^2}{\left((\lambda_{\odot} - \lambda_{\odot}^{\max})^2 + (W/2)^2 \right)} \tag{4}$$

where $\lambda_{\odot}$ and W are expressed in degrees. W is the full-width-half-maximum and $\mathrm{ZHR}^{\max}$ is the peak rate at peak solar longitude $\lambda_{\odot}^{\max}$. The mathematical expression for $N_{6.5}$ is [52]

$$N_{6.5} = n_{6.5} \frac{\chi}{\chi - 1} = n_0 \, \chi^{6.5} \frac{\chi}{\chi - 1} \tag{5}$$

where n_M is the number of incident meteoroids per unit time of magnitude M [52, 54]. Modifying Equation (15) in [28], n_0 is computed as

$$n_0 = \frac{\text{ZHR}\ \ (0.4 + 0.6\chi)\ \ A_{\oplus,\perp}}{(\sum_i P(M_i)\chi^{M_i})\ \ 3600\ \ A_{\text{Eff}}}. \tag{6}$$

In Equation (6), $A_{\oplus,\perp} = \pi R_\oplus^2$ is the cross sectional area of the Earth computed with the modified radius $R_\oplus = R_{\oplus,\text{real}} + h_{\text{atm}}$, where h_{atm} is the atmospheric altitude. A_{Eff} is the effective surface area of observation defined and computed as in [28]. 3600 is used to convert ZHR from rater per hours to rate per seconds. $(0.4 + 0.6\chi)$ is used to correct from apparent magnitude to absolute magnitude [28]. $P(M)$ is the probability function at absolute magnitude M used to consider that only a fraction of meteoroids is observed by a visual standard observer [52, 54]. The set of probability coefficients used comes from [53]. The result is the number of meteoroids impacting the Earth with absolute magnitude 0 per unit time. ZHR is computed through Equation (4), where individual values of ZHR_{max} and W for each meteor shower are randomly drawn from two different Gaussian distributions truncated to the interval $[\max(\mu - 5\sigma, 0), \mu + 5\sigma]$. The first distribution is centered at mean μ_{ZHR} and has standard deviation σ_{ZHR}. The second distribution is centered at μ_W and has standard deviation σ_W. The numerical values μ_{ZHR}, σ_{ZHR}, μ_W, and σ_W for each individual shower are reported in the catalog (see Table 7 in Appendix A).

When targeting the Moon, the number of impacting meteoroids has to be scaled [1, 6, 39]. The scaling is performed with two coefficients, f_1 and f_2 (see Appendix B), which multiply the final result and the kinetic energy, respectively. The number of impacting meteoroids scaled to the Moon is computed as

$$\mathcal{N}_{\text{☾}} = f_1 \int_{t_i - \frac{\Delta t}{2}}^{t_i + \frac{\Delta t}{2}} N_{6.5} \left(\frac{2 f_2 \text{KE}_{\text{min}}}{V_{\text{imp},\oplus}^2 m_{6.5}} \right)^{1-s} \text{d}t. \tag{7}$$

3.3 Impact descriptors

Impact time epoch. The impact time epoch is drawn from a uniform distribution bounded between $-\Delta t/2$ and $\Delta t/2$ for each interval centered at t_i, where Δt and t_i are the time step and the i-th epoch introduced in Section 3.1. A random selection might seem physically incoherent as impacts are not uniformly distributed in time. However, if Δt is sufficiently small (equal or smaller than one hour) the error is negligible.

Impact kinetic energy. The impact kinetic energy is randomly generated through a Pareto distribution with shape parameter (or tail index) $\alpha = (s - 1)$, and scale parameter KE_{min}. The Pareto distribution is a power-law probability distribution which suits the random generation of kinetic energy. The proof of the latter assertion

is shown in Appendix C.

Geocentric velocity. The geocentric velocity (defined at the Earth–Moon system sphere of influence) is a characteristic of the meteor shower and, consequently, of the meteoroid stream. The geocentric velocity V is assumed equal to the average shower geocentric velocity reported in the catalog (see Appendix A, Table 7).

Impact location. The computation of the impact location when targeting the Moon requires a correction of the radiant direction. The procedure takes into account the revolution and relative velocity of the Moon with respect to the Earth.

In the literature, radiant directions are known with a certain degree of uncertainty. They are typically described in terms of mean and standard deviation of both right ascension RA and declination DEC. The radiant direction is drawn from a multivariate Gaussian distribution, assuming RA and DEC uncorrelated. The Gaussian multivariate distribution is centered at the mean values of RA and DEC, with diagonal covariance matrix. The mean values μ_{RA} and μ_{DEC}, and the standard deviations σ_{RA} and σ_{DEC} are reported in Table 7. The diagonal covariance matrix being $\mathbf{\Sigma}_{\mathrm{STR}} = \mathrm{diag}(\sigma_{\mathrm{RA}}^2, \sigma_{\mathrm{RA}}^2)$, where $\mathrm{diag}(\cdot)$ is the operator to build a diagonal matrix from a vector. Resulting RA and DEC are wrapped between $[0, 2\pi]$ and $[-\pi/2, \pi/2]$, respectively.

Starting from the drifting rates $\frac{\Delta(\cdot)}{\Delta\lambda_\odot}$ reported in Table 7, the drifted RA and DEC are computed as $(\cdot) = (\cdot)_{\max} + \frac{\Delta(\cdot)}{\Delta\lambda_\odot}(\lambda_\odot - \lambda_{\odot,\max})$, where the subscript 'max' refers to quantities at the maximum activity period of the shower. The symbol $(\cdot)$ has to be replaced with either RA or DEC. Then, RA and DEC are converted from spherical to Cartesian coordinates[1]. Lastly, the radiant direction is corrected as follows [6]: i) retrieve the Moon velocity vector $\mathbf{V}_{\leftmoon}$ with respect to the Earth–Moon barycenter through SPICE; ii) compute the meteoroid geocentric velocity vector as $\mathbf{V} = -V\mathbf{r}_{\mathrm{rad}}$ where $\mathbf{r}_{\mathrm{rad}}$ is the radiant direction; iii) derive the corrected meteoroid velocity vector $\tilde{\mathbf{V}} = \mathbf{V} - \mathbf{V}_{\leftmoon}$; iv) calculate the corrected radiant direction $\tilde{\mathbf{r}}_{\mathrm{rad}} = -\tilde{\mathbf{V}}/\|\tilde{\mathbf{V}}\|$.

Knowing the radiant direction, the impact location can be computed. Meteoroids may impact any point of the Moon hemisphere facing the radiant direction [6, 32, 33]. Following the procedure in [32], meteoroids are assumed to strike the Moon with a homogeneous distribution on planes perpendicular to the radiant directions.

The zenith attraction, also known as gravitational deflection, is negligible for high velocities [32, 34]. In this work, it is neglected since the number of meteoroids with relatively low geocentric velocity is small, particularly among those belonging to meteoroid streams. Differently, the zenith attraction should be taken into account

[1] Alternatively, the radiant drift can be estimated via the proper motion. Note that a cos(DEC) factor must be considered in the RA radiant shift when calculating the proper motion.

for slow meteoroids because changes in radiant direction may be large in such case.

Moon side of the impact (day or night). Knowing the local time of the impact, it is possible to check whether impacts occur on the illuminated side of the Moon or not. While impacts on the day side are almost impossible to detect, it may be equally harsh to detect meteoroids impacting in the night side but close to the terminator line. Even though there is no atmosphere in space, so making light diffusion much smaller, diffusion still occurs when the light is reflected by the Moon surface (e.g., due to surface features and physical properties). The latter is particularly true when LUMIO is far from the Moon and the terminator is close to the shadowed lunar limb. Therefore, a threshold is introduced to check if the impact location is further than a certain distance from the terminator line. In general, the threshold can be set to zero if there is no need to exclude a priori impacts close to the terminator line.

A threshold distance from the terminator line equal to $d_{\text{trm}} = 50\,\text{km}$ is assumed. Such distance corresponds to the 0.46% of the Moon circumference at the equator. This distance is converted in an angular measure δ according to

$$\delta = \frac{d_{\text{trm}}}{R_{\leftmoon}}. \tag{8}$$

Then, the quantity $l = \cos\left(\delta + \frac{\pi}{2}\right)$ is computed. If the scalar product between the Sun pointing vector and impact location direction is lower than the threshold l, the impact is considered detectable.

Obstruction of visibility. In [20, 31], the number of impacts effectively detectable is assumed to be 50% of the total. This is due to shadowing effects of lunar mountains. In this study we assume an obstruction of 20% because of the larger distances of LUMIO from the Moon with respect to the low-orbiting lunar satellite considered in [31].

Impact velocity. The impact velocity on the lunar surface is computed starting from the geocentric velocity, correcting the velocity for the relative motion of the Moon with respect to the Earth, and considering the gravitational acceleration of the Moon and the Earth, the latter at Moon distance. This is akin to the procedure in [1]. The complete procedure is detailed in Appendix B.

Mass. The mass of a meteoroid is computed inverting the kinetic energy expression

$$\text{KE} = \frac{1}{2}\, m\, V_{\text{imp}}^2 \tag{9}$$

where V_{imp} is the impact velocity on the Moon.

Luminous efficiency. The luminous efficiency η is retrieved exploiting the correlation derived in [36] and experimentally confirmed in [35]

$$\eta = C\ e^{-\left(\frac{V_C}{V_{\text{imp}}}\right)^2} \tag{10}$$

where $C = 1.5 \times 10^{-3}$ is a scaling factor with standard deviation equal to the 10% of the mean. The term $V_C = 9.3\,\text{km}\,\text{s}^{-1}$ is named characteristic velocity and its standard deviation is the 10% of the mean [36]. In Equation (10), the impactor velocity V_{imp} is expressed in $\text{km}\,\text{s}^{-1}$. In our method, C and V_C are randomly generated for each impact from Gaussian distributions using the corresponding means and standard deviations.

Bulk density. For rocky objects the bulk density is drawn from a truncated Gaussian distribution. Mean and standard deviation are reported in the catalog. The lower bound is assumed equal to $1500\,\text{kg}\,\text{m}^{-3}$, while the upper bound is assumed equal to $3500\,\text{kg}\,\text{m}^{-3}$.

On the other hand, when there is a lack of information in the catalog, a bi-modal distribution is used to describe rocky or iron objects. For rocky objects the mean value $1800\,\text{kg}\,\text{m}^{-3}$ and a standard deviation equal to $300\,\text{kg}\,\text{m}^{-3}$ is used [25]. For iron objects the assumed mean is $7370\,\text{kg}\,\text{m}^{-3}$ [55], with a standard deviation equal to the 10% of the mean. The draws of the bi-modal distribution are limited between $[1500, 7874]\ \text{kg}\,\text{m}^{-3}$. The upper bound corresponding to iron density.

Impact angle. The impact angle γ is measured with respect to the local horizon, which means that if $\gamma = 90\,\text{deg}$, then a meteoroid impacts perpendicularly on the lunar surface. Conversely, a meteoroid hits the surface almost horizontally for small impact angles. In this work, the lunar surface is not assumed flat, therefore the impact angle cannot be retrieved from the radiant direction and the impact location. Typically, the impact angle is assumed equal to 45 deg in the literature [6]. In our model, the impact angle is drawn from a truncated Gaussian distribution with mean 45 deg and standard deviation 15 deg. The distribution is truncated in the range $[20, 90]\,\text{deg}$. By assumption, grazing impacts are considered extremely rare, therefore the choice of the lower bound.

Crater diameter and radius. To estimate the crater radius created by the impact Gault's scaling law is exploited [37, 38]. The law is valid up to craters' diameters equal to 100 m. The formulation is [56]

$$D = 0.25\ \rho_p^{0.167}\ \rho_t^{-0.5}\ g^{-0.165}\ (\text{KE})^{0.29}\ \sin(\gamma)^{\frac{1}{3}}. \tag{11}$$

In the formula, D is the diameter in m; ρ_p and ρ_t are the projectile (meteoroid) and target (Moon's surface) bulk density in $\mathrm{kg\,m^{-3}}$, respectively; g is the gravity acceleration; KE is the kinetic energy in J; γ is the impact angle. Target bulk density ρ_t has been assumed equal to $1500\,\mathrm{kg\,m^{-3}}$ [5, 16].

[16] claims that it is not clear if the output diameter of Gault's law is the apparent or rim-to-rim diameter. The rim-to-rim diameter is larger then apparent one up to 30% [16]. However, Gault's law is written for the apparent diameter in [38], which is also confirmed in [16].

If Equation (11) returns a diameter greater than 100 m, the output is discarded and the law developed by Holsapple [57], to get rim-to-rim radius of vertical impacts, is exploited instead. The formulation is [16]

$$R = 10.14\ G^{-0.17}\ a^{0.83} V^{0.34} \tag{12}$$

where R is in m, G is the gravity acceleration in units of Earth's gravity acceleration, a is the impactor radius in m, and V is the impactor speed in $\mathrm{km\,s^{-1}}$. The impactor radius is computed assuming a spherical shape of the meteoroid. The relation does not take into account the possibility of non-vertical impacts. To overcome that limitation, the same dependence on γ of Equation (11) can be used, as done in [16]. A coefficient is introduced to correct the dimension since the output is not the apparent radius. The rim-to-rim radius is assumed 20% larger than the apparent one. Hence, the formula used is

$$R = \frac{10.14}{1.2}\ G^{-0.17}\ \left(\frac{3m}{4\pi\rho_p}\right)^{\frac{0.83}{3}}\ V^{0.34}\ \sin(\gamma)^{\frac{1}{3}} \tag{13}$$

Plume area. According to [56], the plume area is proportional to the crater surface. The coefficient that correlates the two quantities is indicated with β. In our approach, the value of β is chosen randomly from a uniform distribution bounded in [4, 25]. Then, the plume area is obtained through the relation

$$A_p = \beta\pi R^2 \tag{14}$$

where R is the crater radius. In [56], Gault's scaling law [37, 38] is used to estimate the crater diameter, which according to [16] gives an estimate of the apparent crater diameter. Therefore, for consistency, the apparent diameter is used also when relying on a different scaling law.

Apparent magnitude at Earth distance. In [6], an exponential law to correlate the impact flash duration and the apparent magnitude of lunar impact flashes at Earth distance is derived. A similar exponential dependence was found also in [56].

The law is [6]

$$\tau = Ae^{-bm} \tag{15}$$

where τ is the impact flash duration in s, A is the first coefficient, b the second coefficient, and m is the apparent magnitude at Earth distance. These coefficients are expressed in terms of mean and standard deviation. Regarding A, $\mu_A = 77.6\,\mathrm{s}$ and $\sigma_A = 34.4\,\mathrm{s}$, while for b, $\mu_b = 0.94$ and $\sigma_b = 0.06$ [6]. The standard deviation of A is about 44% of the mean. When using such value to randomly select A, results are widely spread. In particular, for some combinations of A and b, meteoroid impacts with low impact energies result in very bright flashes, which is generally unreasonable considering the linear dependence (through the luminous efficiency η) of the impact kinetic energy fraction resulting in radiation emitted in the $[400, 900]\,\mathrm{nm}$ range by an impact. That happens when both A and b are smaller than their means, and A is randomly selected small (but positive), which may occur frequently with the nominal standard deviation σ_A. To solve this issue, which is a limit of the methodology, $\sigma_A = 0.1\mu_A$ is used such that results are narrowed while still keeping a statistical variability.

The values of A and b from Equation (15) are generated randomly from two different truncated Gaussian distributions employing the aforementioned means and standard deviations. Both distributions are defined in the range $(0, +\infty)$, to preserve the physical meaning (τ must be positive) and the trend (τ decreases for fainter impacts).

τ and m are both unknown in Equation (15), as a consequence, a second relation is needed to solve for them. The required equation is derived linking the apparent magnitude with the emitted power of an impact. The result is an equation that can be solved analytically for the apparent magnitude m. Then, m is used to compute τ by means of Equation (15).

The radiated power from a source of apparent magnitude m can be computed through [6]

$$P = F_0 10^{-\frac{m-m_0}{2.5}}\ f\pi d^2\ \Delta\lambda \tag{16}$$

where P is the radiated power in W and $F_0 = 1.369\,49 \times 10^{-10}\,\mathrm{W\,m^{-2}\,m^{-1}}$ is the flux density of a reference source of magnitude $m_0 = 21.1$. The latter values are taken from [6] according to the ones given in [58]. f is the degree of anisotropy of the light emission, d is the distance of the observer from the source, and $\Delta\lambda$ is the bandwidth of interest. The degree of anisotropy depends on the location from which the light is emitted. In our method, $f = 3$ is used as in [51]. The considered bandwidth ranges from 400 nm to 900 nm [51]. This is because the radiated power is compared with the portion of emission over which the luminous efficiency η is computed [51]. When dealing with lunar impact flashes, the distance $d = d_{\oplus\leftmoon}$ is time dependent. However, Equation (16) is used in combination with Equation (15) to obtain τ, which is a peculiar characteristic of the flash itself and should not

depend on the observer distance. Therefore, in Equation (16), the Earth–Moon time-averaged distance is used [59].

The radiated power is expressed in terms of kinetic energy and impact flash duration. In [60], it is remarked that impact flashes exhibits an exponential intensity decay in time. Therefore, to model such behavior, it is assumed an exponential law like

$$P(t) = P_0 \, e^{-\frac{5t}{\tau}}. \tag{17}$$

At the end of the impact flash duration, the emitted power is so small that it is considered negligible. The power used in the left hand side of Equation (16) is the peak power, which corresponds to the peak apparent magnitude registered.

The peak power P_0 is obtained linking the impact kinetic energy with the radiated energy. Then, the radiated energy is computed integrating $P(t)$ over the whole impact flash duration. The integration gives

$$E_r = \int_0^\tau P(t)\mathrm{d}t = P_0 \int_0^\tau e^{-\frac{5t}{\tau}}\mathrm{d}t = \frac{\tau P_0}{5}\left(1 - e^{-5}\right) \approx 0.9933\frac{\tau P_0}{5} \tag{18}$$

where E_r is the radiated energy computed through the luminous efficiency η.

Rearranging the equations, the following relation is obtained

$$\frac{5\eta \mathrm{KE}}{Ae^{-bm}\left(1 - e^{-5}\right)} = F_0 \, 10^{-\frac{m-m_0}{2.5}} \, f\pi d_{\oplus\leftmoon}^2 \, \Delta\lambda_\eta \tag{19}$$

where $\Delta\lambda_\eta = 900 - 400\,\mathrm{nm}$. Equation (19) can be solved analytically for m, which is the only unknown.

Impact flash duration. The impact flash duration is computed exploiting Equation (15), substituting the value of apparent magnitude at the Earth distance computed through Equation (19). The coefficients A and b used in Equation (15) are the ones drawn when deriving the apparent magnitude.

Equivalent black body temperature of radiating plume. The equivalent black body temperature associated to the plume of ejecta particles generated by the impact is computed integrating the spectral emissive power of the black body over the $[400, 900]\,\mathrm{nm}$ spectrum and computing the average impact radiated power.

The spectral emissive power $L(\lambda, T)$, the rate at which radiation of wavelength λ is emitted in all directions per unit wavelength interval $\mathrm{d}\lambda$ about λ and per unit surface area, is defined as

$$L(\lambda, T) = \frac{2\pi hc^2}{\lambda^5\left(e^{\frac{hc}{\lambda k_B T}} - 1\right)} \tag{20}$$

where h is the universal Planck's constant, c is the speed of light in vacuum, and k_B is the universal Boltzmann's constant.

Integrating Equation (20) over the $[400, 900]$ nm spectrum, and multiplying the result by the ejecta plume area gives the impact radiated power. The equivalent black body temperature of the plume decreases over time, due to the ejecta cooling down. However, we assumed a constant equivalent black body temperature T since the impact dynamics is not modeled.

The integral of the emissive power multiplied by plume area is equated to the average radiated power of the impact. Then, T is numerically computed from the following implicit relation

$$A_p \int_{\lambda_1}^{\lambda_2} L(\lambda, T) \mathrm{d}\lambda - \frac{\eta \mathrm{KE}}{\tau} = 0 \tag{21}$$

where the integration extremes are $\lambda_1 = 400\,\mathrm{nm}$ and $\lambda_2 = 900\,\mathrm{nm}$ [51]. The temperature T is the only unknown of the equation. The retrieved temperature is not the peak temperature of the impact flash. Indeed, it is obtained using the average radiated power $\bar{P}$ and not the peak power P_0.

3.4 Summary of the procedure

The procedure developed for the generation of an individual meteoroid belonging to a stream is outlined in Figure 3. The methodology produces a set of descriptors (red boxes) that can be analyzed a posteriori. Part of the science requirements for the LUMIO lunar CubeSat are inferred from inspection of these descriptors.

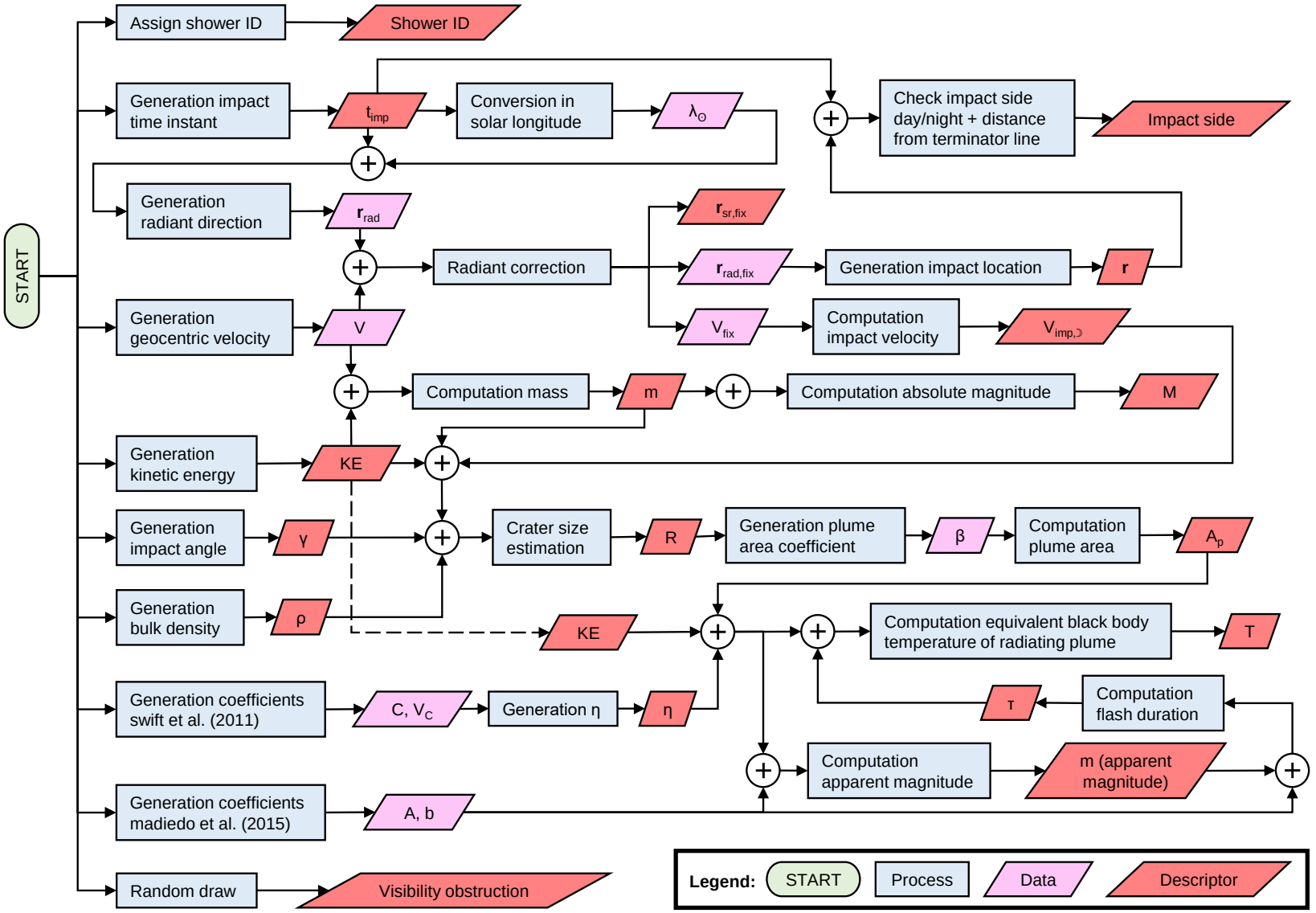

Figure 3: Schematic representation of meteoroid stream impact generation when targeting the Moon.

4 Modeling of sporadic background

The first steps of the generation procedure of sporadic meteoroids are different with respect to meteoroid streams. The steps followed in sampling the sporadic background population are depicted in Figure 4.

4.1 Number of meteoroids to generate

The number of meteoroids for each individual sporadic source, impacting Earth, and with kinetic energy higher than $\mathrm{KE}_{\mathrm{min}}$ is

$$\mathcal{N}_{\oplus} = \int_{t_0}^{t_f} N_{6.5} \left(\frac{2\mathrm{KE}_{\mathrm{min}}}{V_{\mathrm{imp},\oplus}^2 m_{6.5}} \right)^{1-s} \mathrm{d}t \tag{22}$$

where the extremes of integration are t_0 and t_f. To compute $\mathcal{N}_{\oplus}$ by means of Equation (22) some quantities are needed: $N_{6.5}$, $m_{6.5}$, $V_{\mathrm{imp},\oplus}$, and s. The impact velocity at Earth $V_{\mathrm{imp},\oplus}$ is derived from the source geocentric velocity reported in the catalog (see Table 8). $m_{6.5}$ is computed through Equation (3). s is obtained from χ by means of Equation (2). For all the sources of the sporadic background, the population index χ is drawn from a truncated Gaussian distribution bounded in $(0, +\infty)$, having mean $\mu_\chi = 3.03$ and standard deviation $\sigma_\chi = 0.13$ [13].

$N_{6.5}$ is computed through Equation (5). Adapting to the sporadic background Equation (15) in [28], n_0 is given by

$$n_0 = \frac{\mathrm{HR_i} \ (0.4 + 0.6\chi) \ A_{\oplus,\perp}}{(\sum_i P(M_i)\chi^{M_i}) \ 3600 \ A_{\mathrm{eff}}} \tag{23}$$

where $\mathrm{HR}_i = S_i \mathrm{HR}(\lambda_\odot)$ depends on the solar longitude $\lambda_\odot$. It is the characteristic hourly rate of the i-th sporadic source estimated multiplying the relative strength S_i (see Table 8) with the sporadic hourly rate $\mathrm{HR}(\lambda_\odot)$. The latter is linearly interpolated from the observational data provided in [50] and here reported in Table 9. The number of meteoroids is scaled to the Moon in a similar fashion as done for meteoroid streams (see Section 3.2).

4.2 Impact descriptors

Impact time epoch. The time epoch of the impact is drawn randomly from the probability density function derived from the hourly rate $\mathrm{HR}(\lambda_\odot)$ bounded in $[t_0, t_f]$.

Geocentric velocity. The geocentric velocity is drawn from a proper velocity distribution. The velocity distributions reported in [45] have been used for this study. The ST is assumed symmetric to the NT, therefore the same velocity distribution has been used for both. The average values of the distributions are reported in Table 8.

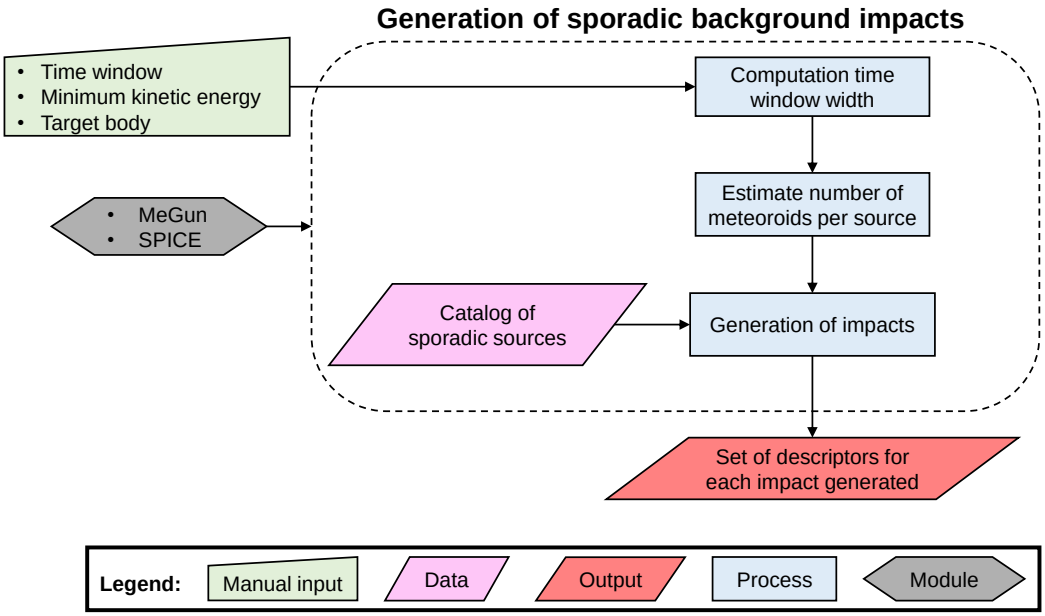

Figure 4: Schematic representation of the generation procedure for sporadic background impacts.

Impact location. The radiant direction in terms of the ecliptic longitude λ and latitude β is drawn from a multivariate Gaussian distribution, assuming λ and β uncorrelated. The mean values μ_λ and μ_β, and the standard deviations σ_λ and σ_β are taken from Table 8 (see Appendix A). The diagonal covariance matrix being $\mathbf{\Sigma}_{\mathrm{SPO}} = \mathrm{diag}(\sigma_\lambda^2, \sigma_\beta^2)$. Then, the radiant direction is corrected as done for meteoroid streams in Section 3.3. The impact location is generated following the procedure developed in [32] and already applied to the modeling of meteoroid streams.

Other descriptors. Regarding the computation of the other descriptors, the same assumptions and methodology employed in the modeling of meteoroid streams apply also to the sporadic background. In the sporadic background catalog the following information are missing: population index, hourly rate, and bulk density. The first two have already been discussed. About the latter, $\mu_\rho = 1800\,\mathrm{kg\,m^3}$ and $\sigma_\rho = 300\,\mathrm{kg\,m^{-3}}$ are used when generating the bulk density of a sporadic meteoroid [25].

4.3 Summary of the procedure

Figure 5 shows a schematic representation of the steps performed to generate a sporadic impact. As for meteoroid streams, the methodology returns a number of descriptors from which part of the science requirements of the LUMIO mission have been inferred.

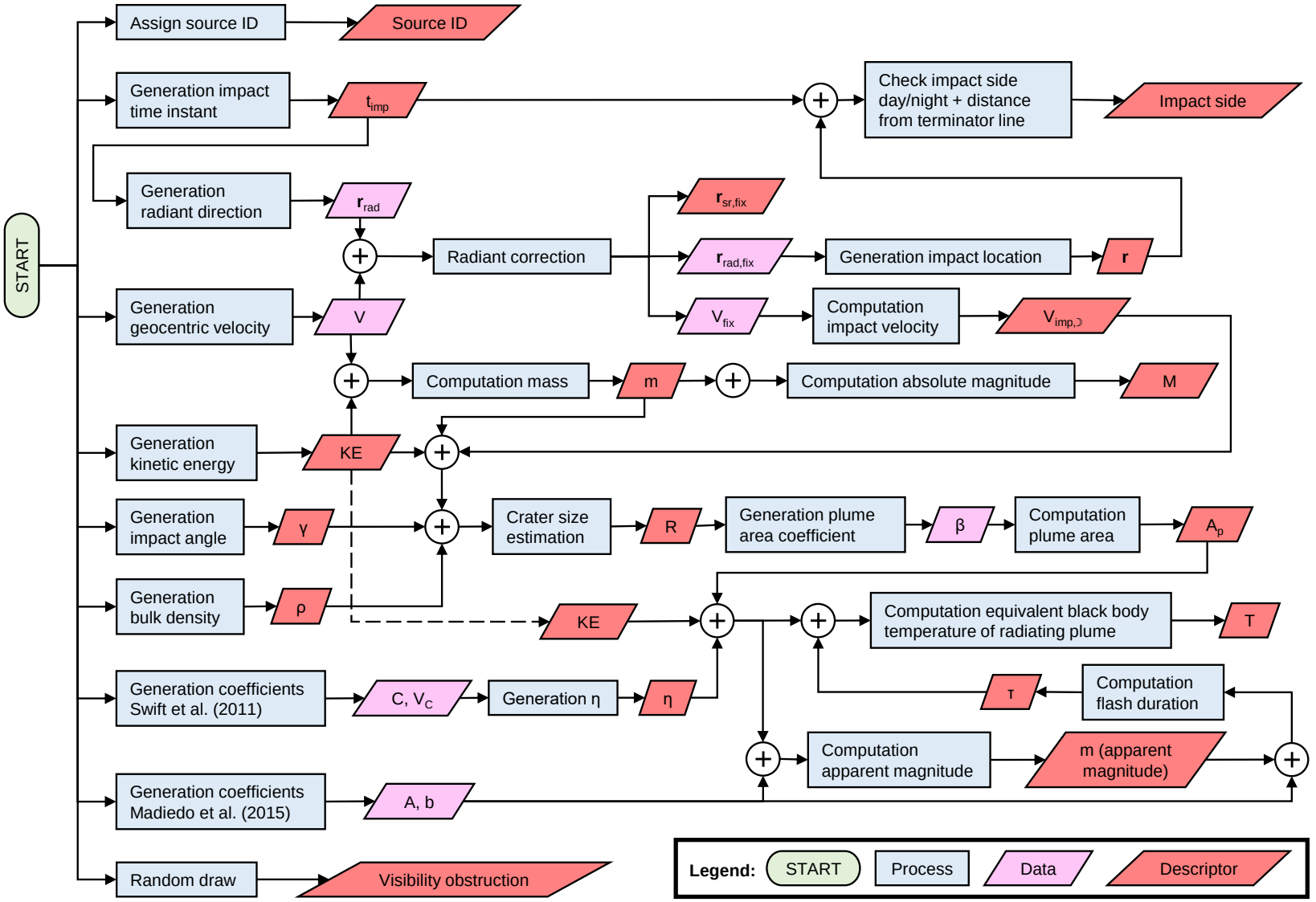

Figure 5: Schematic representation of sporadic impact generation when targeting the Moon.

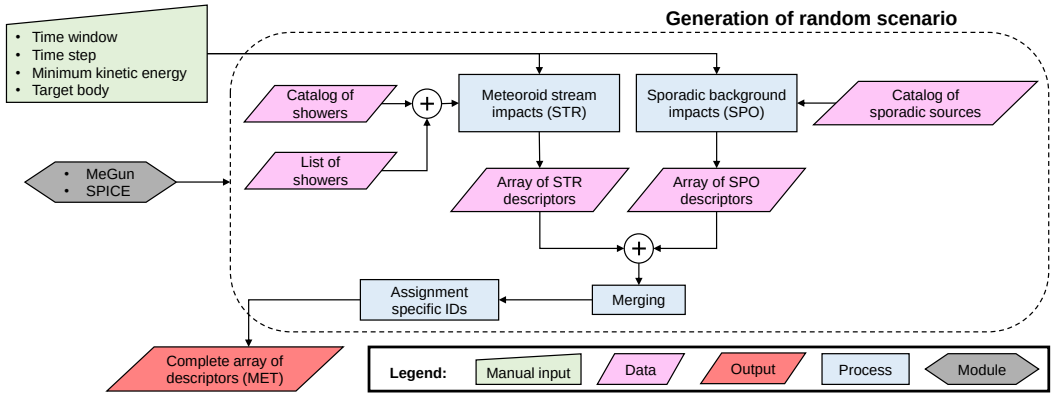

Figure 6: Schematic representation of the overall generation of a scenario.

5 Summary of meteoroid impacts modeling

The flowchart in Figure 6 provides an overview of the overall modeling procedure. MeGun takes as inputs a time window, a time step, a minimum kinetic energy, and a target body. It returns a set of descriptors. Generation of meteoroids belonging to streams is independent to that of sporadic impactors.

Modeling of meteoroid streams requires nested loops. The time window is discretized and an array of time epochs is built from it. Next, active showers (then also active streams) are identified for each time interval. The number of meteoroids to produce is computed for the active streams. Impactors are finally simulated and the set of descriptors is returned.

Modeling of the sporadic background includes 6 sources which flux depends on the solar longitude [50]. Even though dependence of sporadic radiant directions on the solar longitude $\lambda_\odot$ is reported in the literature [44, 45, 61], the Gaussian fits of the radiants have been used in this study [45]. The number of sporadic meteoroids per source is determined from the minimum kinetic energy, the relative strength of the source, and the time span. They are generated and the set of descriptors is returned.

Finally, the two sets of descriptors are merged, this is always possible because the two sets contain the same type of information. Table 1 summarizes all the physical parameters introduced, it lists their numerical value and source.

Table 1: Collection of physical parameters.

Parameter	Description	Value	Reference
$\beta_{\max}$	Upper bound of ratio between plume area and crater surface	25	[56]
$\beta_{\min}$	Lower bound of ratio between plume area and crater surface	4	[56]
$\gamma_{\max}$	Maximum impact angle	90 deg	Assumed
$\gamma_{\min}$	Minimum impact angle	20 deg	Assumed
$\lambda_{\text{vis},1}$	Lower wavelength	400 nm	[51]
$\lambda_{\text{vis},2}$	Upper wavelength	900 nm	[51]
μ_γ	Mean impact angle	45 deg	Assumed
$\mu_{\rho,\text{rocky}}$	Mean meteoroid bulk density of rocky impactors for bimodal distribution	$1800\,\text{kg}\,\text{m}^{-3}$	[25]
$\mu_{\rho,\text{iron}}$	Mean meteoroid bulk density of rocky impactors for bimodal distribution	$7370\,\text{kg}\,\text{m}^{-3}$	[55]
$\mu_{\chi,\text{SPO}}$	Mean population index of sporadic background	3.03	[13]
μ_{HR}	Mean HR	$10\,\text{h}^{-1}$	[6, 50]
$\rho_{\max}$	Maximum meteoroid bulk density (iron density)	$7874\,\text{kg}\,\text{m}^{-3}$	Assumed
$\rho_{\min}$	Minimum meteoroid bulk density	$1500\,\text{kg}\,\text{m}^{-3}$	Assumed
ρ_t	Bulk density of lunar regolith (target)	$1500\,\text{kg}\,\text{m}^{-3}$	[5]
σ_γ	Standard deviation of impact angle	15 deg	Assumed
σ_ρ	Standard deviation of meteoroid bulk density for rocky impactors	$300\,\text{kg}\,\text{m}^{-3}$	[25]
$\sigma_{\chi,\text{SPO}}$	Standard deviation of sporadic background population index	0.13	[13]
σ_{HR}	Standard deviation of HR	$1.5\,\text{h}^{-1}$	[50]
$\sigma_{\text{RA,DEC}}$	Standard deviation of meteoroid stream radiant direction if datum is missing	5 deg	Assumed
χ	Population index of meteoroid stream to use as mean if datum is missing	2.5	Assumed
d_{trm}	Minimum distance from terminator line	50 km	Assumed
f	Anisotropy degree of the light emission	3	[51]
$f_{\sigma\mu}$	Ratio between standard deviation and mean if standard deviation is missing	0.1	Assumed
h_{atm}	Atmosphere altitude	100 km	[1]
$V_{\text{imp},\oplus}$	Reference impact velocity at Earth	$20.8\,\text{km}\,\text{s}^{-1}$	[48]
$V_{\text{imp},\oplus,\max}$	Maximum impact velocity at Earth	$72.8\,\text{km}\,\text{s}^{-1}$	[62]
$V_{\text{imp},☾}$	Reference impact velocity at Moon	$17\,\text{km}\,\text{s}^{-1}$	[1, 6, 15, 20]
$V_{\min}$	Minimum geocentric velocity	$0\,\text{km}\,\text{s}^{-1}$	Assumed
W	Full-Width-Half-Maximum of ZHR time dependence law to use as mean for meteoroid streams if datum is missing	2 deg	Assumed
ZHR	ZHR to use as mean for meteoroid streams if datum is missing	$1\,\text{h}^{-1}$	Assumed

Table 2: Setups used for methodology validation.

Setup		Value
Target	-	Moon
Time window beginning	t_i	1 January 2022 12:00:00.0 UTC
Time window ending	t_f	1 January 2027 12:00:00.0 UTC
Time step	Δt	1 h
Min kinetic energy at the Moon	$\mathrm{KE}_{\leftmoon,\mathrm{min}}$	1×10^{-7} kton TNT Equivalent
Min kinetic energy at the Earth	$\mathrm{KE}_{\oplus,\mathrm{min}}$	2.05×10^{-7} kton TNT Equivalent
Stochastic scenarios	N_{scn}	10^3

6 Validation and results

To assess the methodology and to validate our model, a comparison against results reported in the literature has been performed. For this purpose, impact rates of 10^3 stochastic scenarios have been derived. The inputs are collected in Table 2. Each scenario covers a time span of 5 years.

The lunar impact rates generated are shown in Figure 7. In the chart, the meteoroid fluxes from literature are scaled to the Moon. The average scenario, represented by blue diamonds joined with the blue solid line, is close to the impact frequencies reported in the literature [7, 16]. Nonetheless, at low and high impact kinetic energies, a typical scenario yields rates similar to [16].

6.1 Temporal distribution of impacts

The temporal distributions of lunar impacts generated is herewith presented. The setups used to retrieve the temporal distributions are collected in Table 3. Each stochastic scenario covers a time span of 5 years. In these simulations the focus is on the impacts with kinetic energies at Earth in the $[10^{-6}, 10^{-1}]$ kton TNT Equivalent range. The range has been chosen because of interest for the LUMIO mission [20].

The plot in Figure 8 shows the temporal distribution of the lunar impacts. As an example, the temporal distribution of the Geminids meteoroid stream is presented in Figure 9. According to the results, it appears to be among the strongest meteoroid streams, which is expected considering its characteristic ZHR. Finally, the plot of Figure 10 shows the temporal distribution of the lunar impacts belonging to the sporadic background separately. Results in plots of Figures 8, 9, and 10 are represented in 1 deg bins of solar longitude.

The red peak in Figure 9 is caused by the Geminids stream. During the phase A

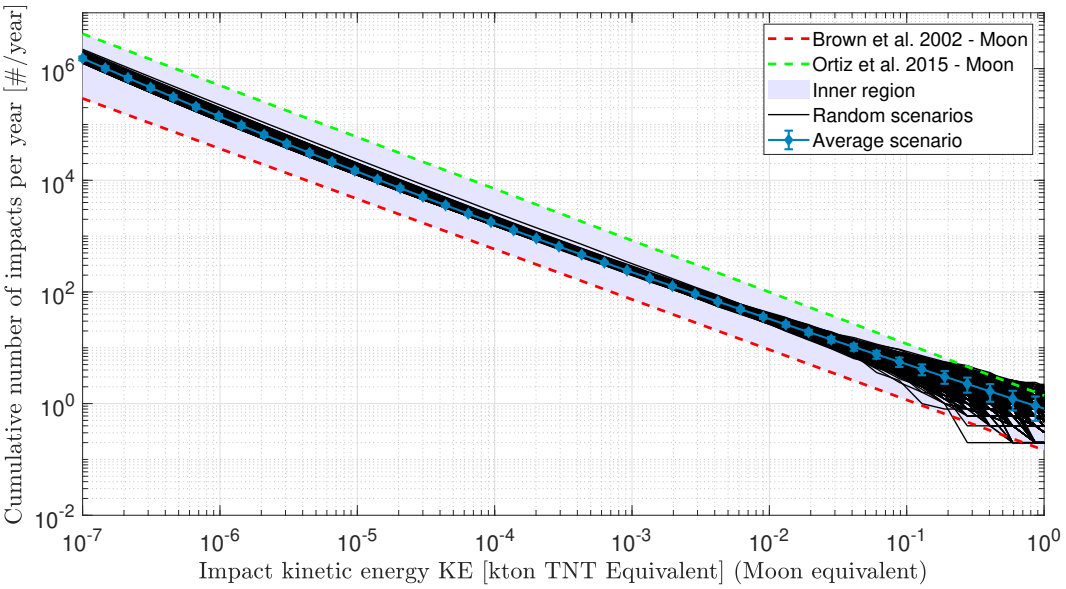

Figure 7: Meteoroid impacts energy distribution. The solid black lines represent the meteoroid fluxes of all the stochastic scenarios that have been generated. The average scenario is indicated by the blue diamonds joined with the blue solid line. The dashed red line and the green line are the impact frequency according to [7] and [16] but scaled to the Moon, respectively. Scenarios cover a time span of 5 years. Results obtained from 10^3 runs.

study of the LUMIO mission, this figure has been used to infer the highest expected daily rate of impacts ascribable to meteoroid streams. Differently, the red curve in Figure 10 has been used to infer the average daily rate of impacts due to the sporadic background.

6.2 Number of observable impacts

To perform an estimation of those impacts potentially observed by LUMIO, some impacts have been filtered out. Specifically, the meteoroids that i) impact the Moon in its illuminated side, ii) impact the Moon in the nearside, iii) are obstructed by features of the lunar surface (see Section 3.3), and iv) impact the Moon when the farside illumination is greater than 50% [15] have been discarded in the analysis.

The scientific return of the resulting temporal distribution is shown in Figure 11. As an example, impacts belonging to GEM are shown in Figure 12, while the temporal distribution regarding the sporadic background is shown in Figure 13. On average, the expected number of impacts per day belonging to the GEM and within the impact kinetic energy range of interest is 1479 at the activity peak. Regarding the sporadic background, the expected number of sporadic impacts per day and in the same energy range is on average 26.

The temporal distribution of the expected scientific return strongly depends on the period in which the observation is performed. The plots in Figure 14 show two significant examples of how the trend of the scientific return changes from year

Table 3: Setups used for computing temporal distribution of impacts and estimating the number of potentially observable impacts.

Setup		**Value**
Target	-	Moon
Time window beginning	t_i	1 January 2022 12:00:00.0 UTC
Time window ending	t_f	1 January 2027 12:00:00.0 UTC
Time step	Δt	1 h
Min kinetic energy at the Moon	$\mathrm{KE}_{\leftmoon,\mathrm{min}}$	7.33×10^{-7} kton TNT Equivalent
Min kinetic energy at the Earth	$\mathrm{KE}_{\oplus,\mathrm{min}}$	1×10^{-6} kton TNT Equivalent
Max kinetic energy at the Moon	$\mathrm{KE}_{\leftmoon,\mathrm{max}}$	7.33×10^{-2} kton TNT Equivalent
Max kinetic energy at the Earth	$\mathrm{KE}_{\oplus,\mathrm{max}}$	1×10^{-1} kton TNT Equivalent
Stochastic scenarios	N_{scn}	10^3

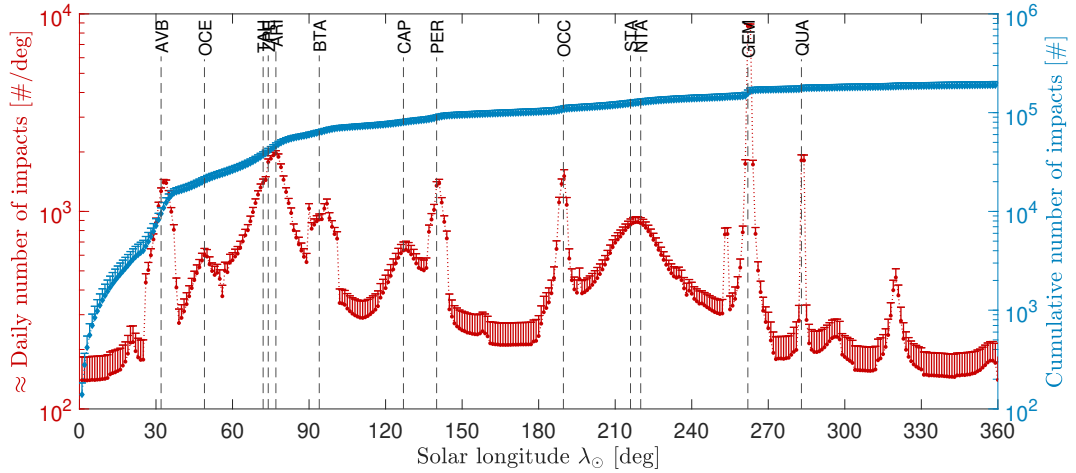

Figure 8: Temporal distribution of lunar meteoroid impacts. On the left y-axis, the number of impacts in 1 deg bins of solar longitude marked by red dots joined with a red solid line. On the right y-axis, the cumulative number of impacts in 1 deg bins of solar longitude marked by blue diamonds joined with a blue solid line. The vertical dashed black lines are the peak solar longitudes of the major streams modeled. Average results of scenarios covering a time span of 5 years wrapped between $[0, 360]$ deg. The number of impacts in bins corresponding to the same $\lambda_\odot$ are summed and divided by 5. KE $\in [10^{-6}, 10^{-1}]$ kton TNT Equivalent, Earth equivalent. Only the upper error bars are plotted, the lower error bars are inferred by symmetry from the upper ones. Results obtained from 1000 runs.

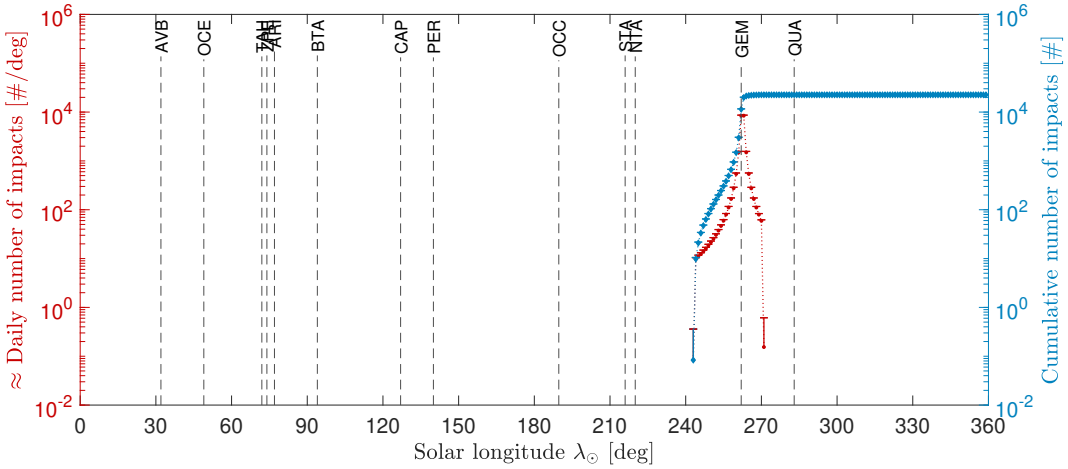

Figure 9: Temporal distribution of GEM lunar impacts. On the left y-axis, the number of impacts in 1 deg bins of solar longitude marked by red dots joined with a red solid line. On the right y-axis, the cumulative number of impacts in 1 deg bins of solar longitude marked by blue diamonds joined with a blue solid line. The vertical dashed black lines are the peak solar longitudes of the major streams modeled. Average results of scenarios covering a time span of 5 years wrapped between $[0, 360]$ deg. The number of impacts in bins corresponding to the same $\lambda_\odot$ are summed and divided by 5. KE $\in [10^{-6}, 10^{-1}]$ kton TNT Equivalent, Earth equivalent. Only the upper error bars are plotted, the lower error bars are inferred by symmetry from the upper ones. Results obtained from 1000 runs.

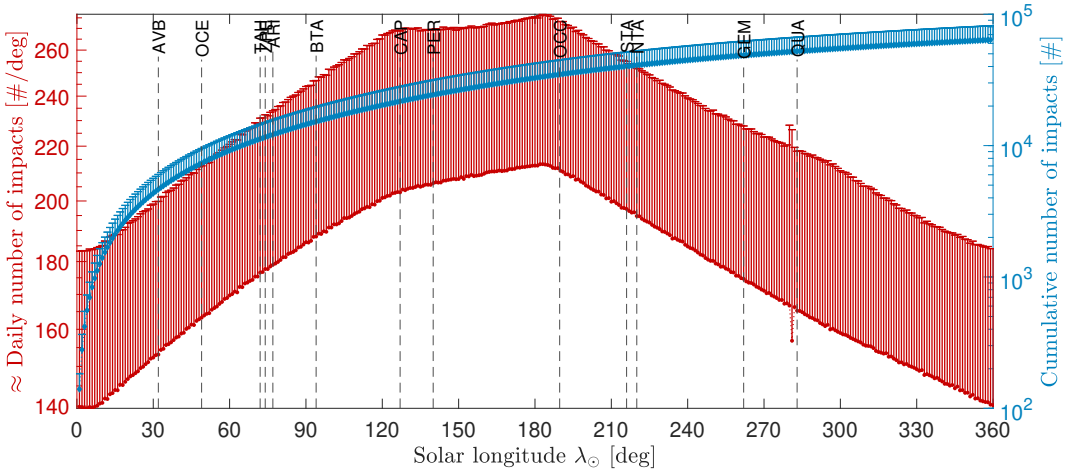

Figure 10: Temporal distribution of sporadic lunar impacts. On the left y-axis, the number of impacts in 1 deg bins of solar longitude marked by red dots joined with a red solid line. On the right y-axis, the cumulative number of impacts in 1 deg bins of solar longitude marked by blue diamonds joined with a blue solid line. The vertical dashed black lines are the peak solar longitudes of the major streams modeled. Average results of scenarios covering a time span of 5 years wrapped between $[0, 360]$ deg. The number of impacts in bins corresponding to the same $\lambda_\odot$ are summed and divided by 5. KE $\in [10^{-6}, 10^{-1}]$ kton TNT Equivalent, Earth equivalent. Only the upper error bars are plotted, the lower error bars are inferred by symmetry from the upper ones. Results obtained from 1000 runs.

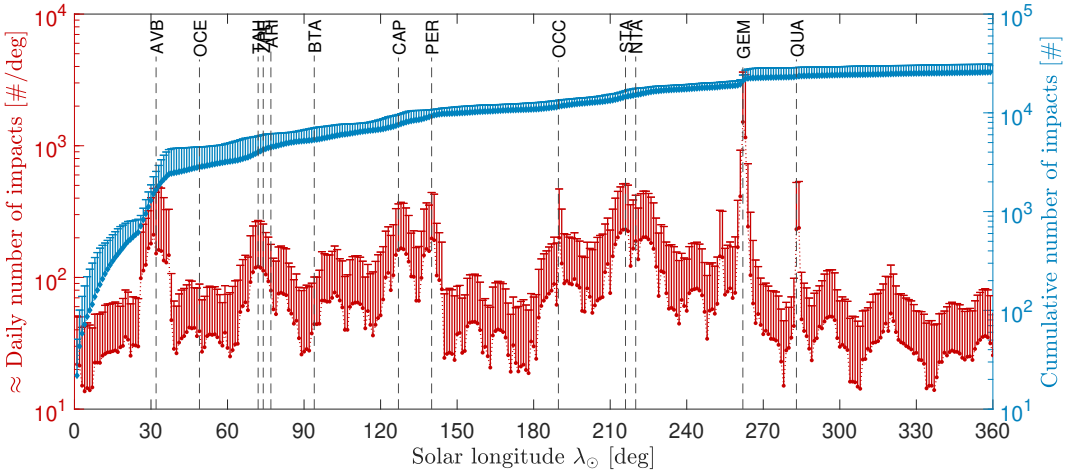

Figure 11: Temporal distribution of the estimated scientific return. On the left y-axis, the number of expected to be detected impacts in 1 deg bins of solar longitude marked by red dots joined with a red solid line. On the right y-axis, the cumulative number of impacts in 1 deg bins of solar longitude marked by blue diamonds joined with a blue solid line. The vertical dashed black lines are the peak solar longitudes of the major streams modeled. Average results of scenarios covering a time span of 5 years wrapped between $[0, 360]$ deg. The number of impacts in bins corresponding to the same $\lambda_\odot$ are summed and divided by 5. KE $\in [10^{-6}, 10^{-1}]$ kton TNT Equivalent, Earth equivalent. Only the upper error bars are plotted, the lower error bars are inferred by symmetry from the upper ones. Results obtained from 1000 runs.

to year. The periodic plateaus visible in the red curves correspond to periods of approximately 14 days where the Moon farside illumination is greater than 50%. As a consequence, no impacts can be detected because LUMIO cannot perform scientific observations in such illumination condition. The aforementioned periodic plateaus shift in time because of the Sun–Earth–Moon orbital geometry. Remarkably, the activity peak of GEM is not overlapped with a plateau during year 2024. Conversely, the GEM activity peak is missed during year 2025.

6.3 Sample scenario: 2024

In this Section, a sample scenario targeting the Moon is presented and discussed. The inputs to generate the scenario are shown in Table 4. The scenario simulates the lunar meteoroid environment in the year 2024.

6.3.1 Individual source contributions

The contribution of individual sources has been drawn in a bar plot[1] The chart is presented in Figure 15, showing the number of impactors on the y-axis. The largest contributions come from the sporadic background sources (HE, AH, NA, SA, NT, and ST). GEM and PER are characterized by a high impact rate. On the contrary, NTA, AVB, and TAH are characterized by a low impact rate. However,

[1] See Appendix A, Table 6 for the correspondence between IAU code and shower name.

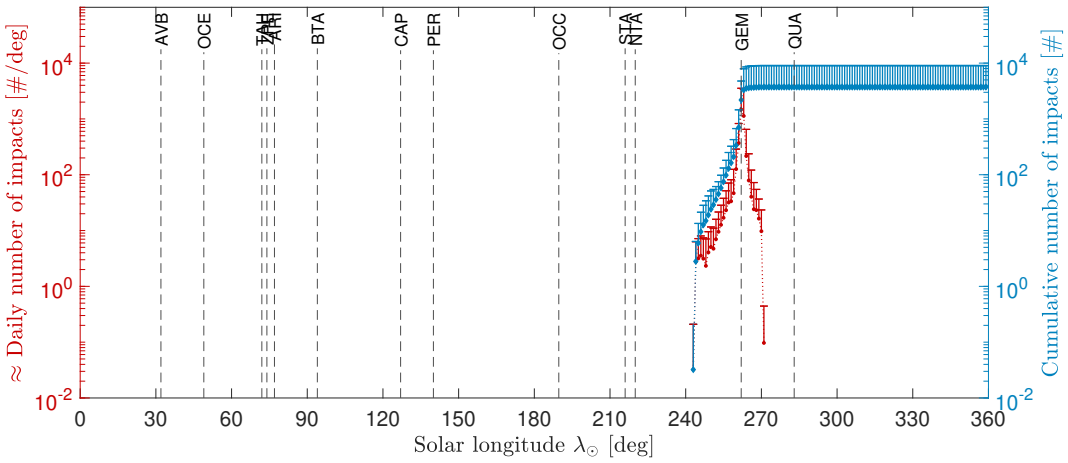

Figure 12: Temporal distribution of the estimated GEM scientific return. On the left y-axis, the number of expected to be detected impacts in 1 deg bins of solar longitude marked by red dots joined with a red solid line. On the right y-axis, the cumulative number of impacts in 1 deg bins of solar longitude marked by blue diamonds joined with a blue solid line. The vertical dashed black lines are the peak solar longitudes of the major streams modeled. Average results of scenarios covering a time span of 5 years wrapped between $[0, 360]$ deg. The number of impacts in bins corresponding to the same $\lambda_\odot$ are summed and divided by 5. KE $\in [10^{-6}, 10^{-1}]$ kton TNT Equivalent, Earth equivalent. Only the upper error bars are plotted, the lower error bars are inferred by symmetry from the upper ones. Results obtained from 1000 runs.

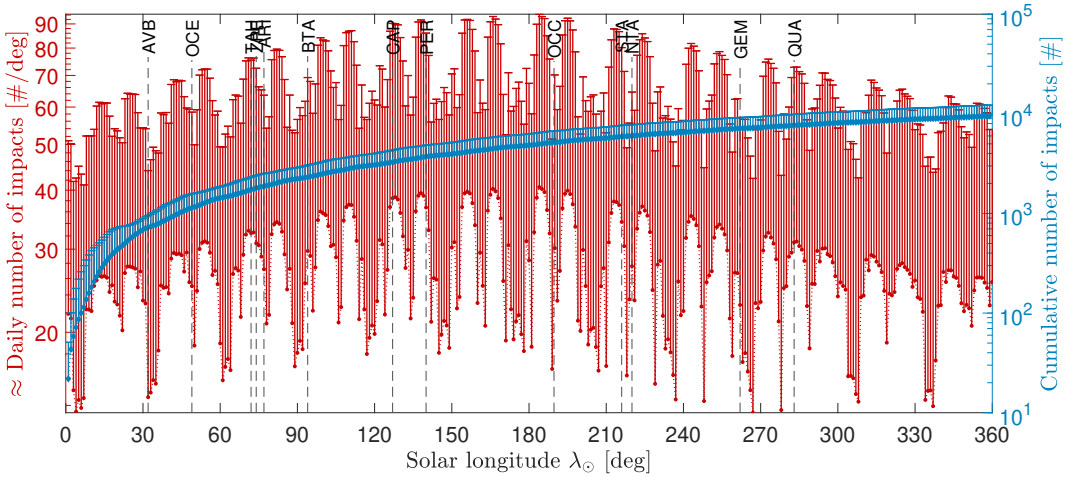

Figure 13: Temporal distribution of estimated sporadic background scientific return. On the left y-axis, the number of expected to be detected impacts in 1 deg bins of solar longitude marked by red dots joined with a red solid line. On the right y-axis, the cumulative number of impacts in 1 deg bins of solar longitude marked by blue diamonds joined with a blue solid line. The vertical dashed black lines are the peak solar longitudes of the major streams modeled. Average results of scenarios covering a time span of 5 years wrapped between $[0, 360]$ deg. The number of impacts in bins corresponding to the same $\lambda_\odot$ are summed and divided by 5. KE $\in [10^{-6}, 10^{-1}]$ kton TNT Equivalent, Earth equivalent. Only the upper error bars are plotted, the lower error bars are inferred by symmetry from the upper ones. Results obtained from 1000 runs.

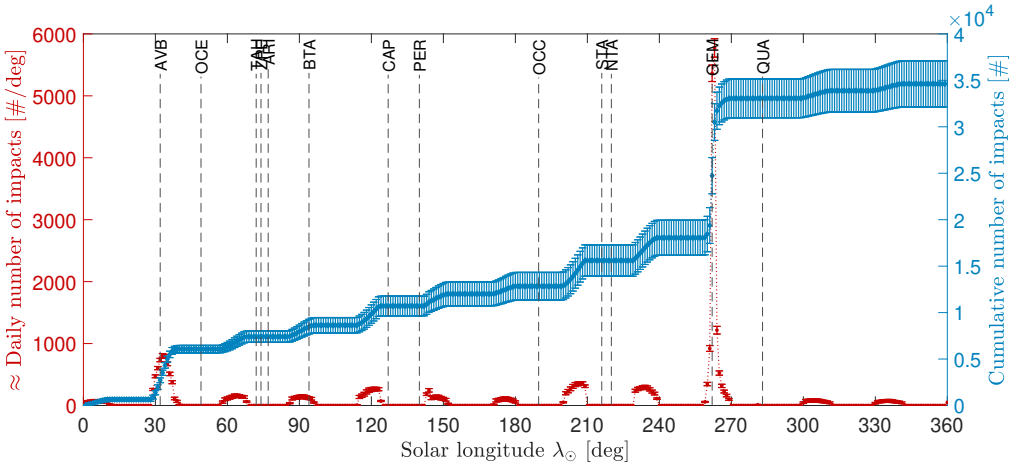

(a) Temporal distribution of the scientific output during year 2024.

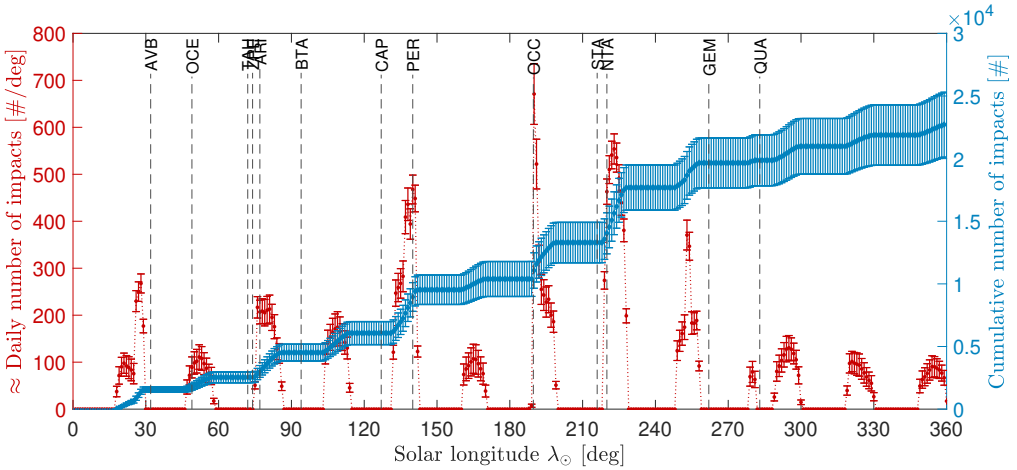

(b) Temporal distribution of the scientific output during year 2025.

Figure 14: Temporal distribution of the estimated scientific output for different years. In the plots, on the left y-axis, the number of expected to be detected impacts in 1 deg bins of solar longitude marked by red dots joined with a red solid line. On the right y-axis, the cumulative number of impacts in 1 deg bins of solar longitude marked by blue diamonds joined with a blue solid line. The vertical dashed black lines are the peak solar longitudes of the major streams modeled. KE $\in [10^{-6}, 10^{-1}]$ kton TNT Equivalent, Earth equivalent. Results obtained from 1000 runs.

Table 4: Inputs to generate the sample scenario.

Setup		**Value**
Target	-	Moon
Time window beginning	t_i	1 January 2024 12:00:00.0 UTC
Time window ending	t_f	1 January 2025 12:00:00.0 UTC
Time step	Δt	1 h
Min kinetic energy at the Moon	$\mathrm{KE}_{\leftmoon,\mathrm{min}}$	10^{-7} kton TNT Equivalent
Min kinetic energy at the Earth	$\mathrm{KE}_{\oplus,\mathrm{min}}$	1.36×10^{-7} kton TNT Equivalent

their contribution is relevant on a yearly basis since their activity period is longer than other showers. Finally, also ARI, ZPE, BTE show relevant contributions. Unfortunately, since they are daytime showers, they are hardly observable with the impact detection methodology implemented in LUMIO.

6.3.2 Impact locations of Geminids and Perseids' meteoroids

The impact locations of the two strongest streams acting in the northern hemisphere are shown.

Geminids (GEM, #4). One of the most prolific streams. The activity period is in the first half of December. The peak is around 14 December

Perseids (PER, #7). It starts in the middle of July and goes on until almost the end of August. The peak is approximately on 12 August.

Two out of the four figures in Figure 16 show the impact locations of the meteoroids belonging to GEM (top-left) and PER (bottom-left). The other two plots show the subradiant points positions of the same impacts belonging to GEM (top-right) and PER (bottom-right). Impacts and subradiant points are represented by red dots. Subradiant points are distributed along strips in the northern hemisphere. On the other hand, impacts are spread over wider regions.

In this scenario, most GEM meteoroids hit the farside, thus, they are potentially detectable by LUMIO but completely missed by Earth-based assets. On the contrary, PER activity peak is in the nearside, where many dots accumulate. In that case only some impacts may be detected by LUMIO, while the majority can be seen from ground-based observatories.

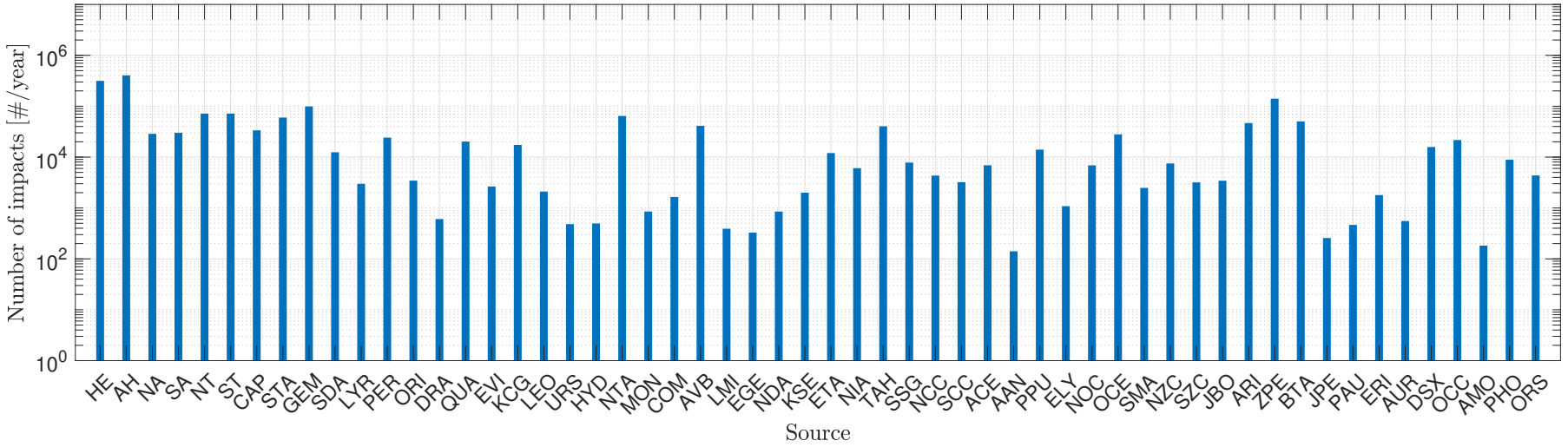

Figure 15: Individual source contributions to the number of lunar impacts in 2024. Number of meteoroids on the y-axis. Bars labeled with showers's IAU codes or sporadic source name tags. KE $\geq 10^{-7}$ kton TNT Equivalent, Moon equivalent. Semi-logarithmic scale plots, logarithmic scale on y-axis.

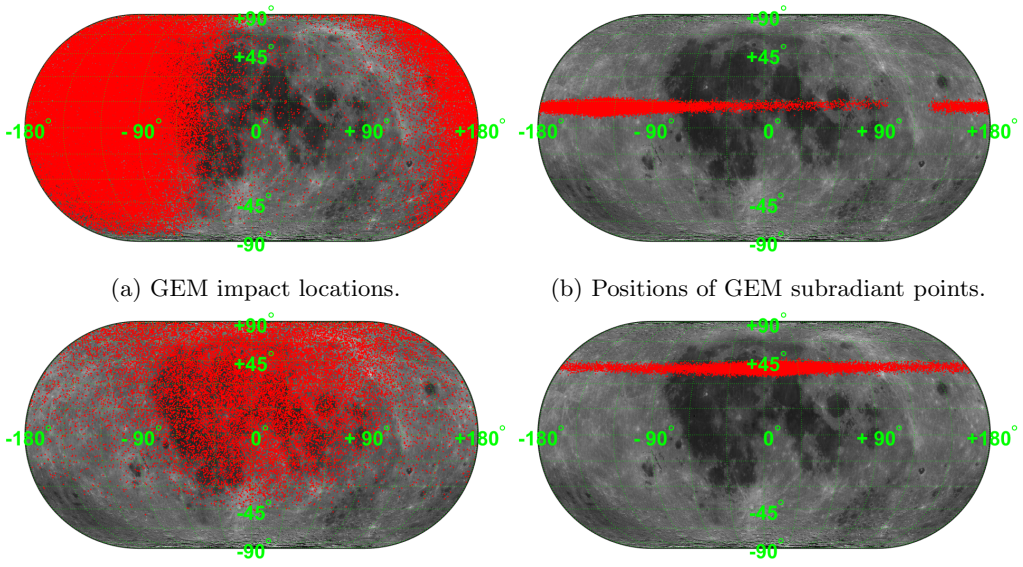

(a) GEM impact locations.

(b) Positions of GEM subradiant points.

(c) PER impact locations.

(d) Positions of PER subradiant points.

Figure 16: Impact locations and subradiant positions of GEM and PER impacting the Moon in 2024. The lunar surface is plotted in the background. KE $\geq 10^{-7}$ kton TNT Equivalent, Moon equivalent.

6.3.3 Impact dynamics

This section presents an analysis of the impact dynamics performed on the sample scenario simulated with our model.

The apparent crater diameter as function of the impact kinetic energy is presented in Figure 17. Values reach tens of m in the case of high energy impacts. Figure 18 shows the area of the plumes raised after the impact plotted versus the impact kinetic energy. High energy impacts are characterized by areas in the order of 10^4 m^2. The square operator and the variability in the selection of the proportionality coefficient β in Equation (14) cause the larger spreading of plume areas with respect to crater diameters.

The plot in Figure 19 presents the apparent magnitudes of impact flashes perceived by an observer looking at the Moon from the Earth. The apparent magnitude is plotted versus the impact kinetic energy. The flash duration as a function of the impact kinetic energy is shown in Figure 20.

Impact flash duration and apparent magnitude are linked through Equation (15). The flash duration is shown as a function of the apparent magnitude in Figure 21. The black solid line superimposed to the tiny blue dots is the correlation reported in [39]. Simulation results and the black solid line are in such agreement as a consequence of the underlying model (see Section 3.3).

Next, in Figure 22, the luminous efficiency is depicted as a function of the meteoroid impact velocity. The blue dots are the efficiencies returned by MeGun. The black

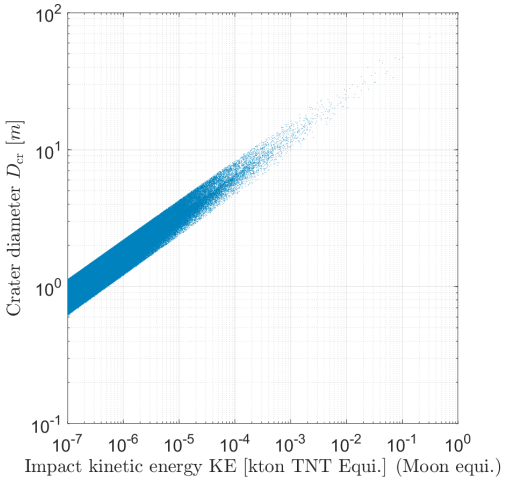

Figure 17: Impact crater diameter of lunar impacts (2024 scenario). The blue dots represent diameter plotted versus impact kinetic energy at the Moon. Log-log scale plot.

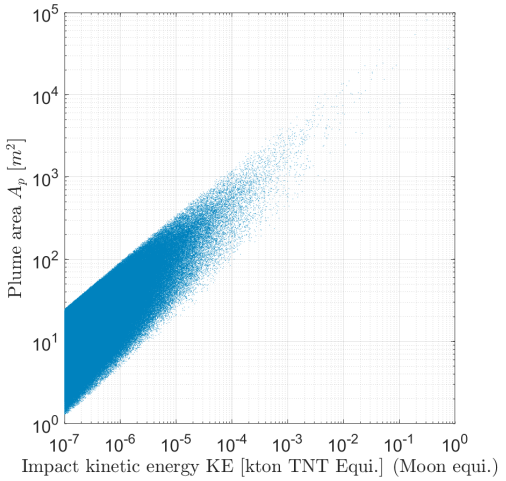

Figure 18: Area of plumes raised by lunar impacts (2024 scenario). The blue dots represent the area as a function of the impact kinetic energy at the Moon. Log-log scale plot.

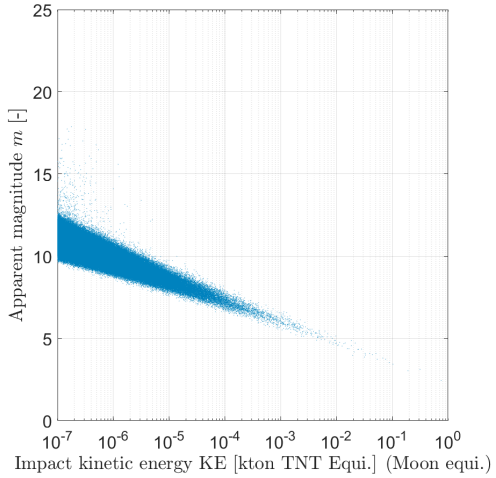

Figure 19: Apparent magnitude of lunar impacts (2024 scenario). The blue dots represent the apparent magnitude perceived by an observer on Earth versus the impact kinetic energy at the Moon. Semi-log scale plot.

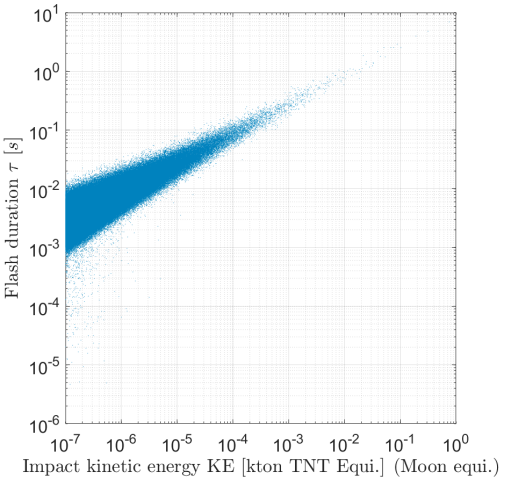

Figure 20: Impact flash duration of lunar impacts (2024 scenario). Duration is represented by the blue dots as a function of impact kinetic energy at the Moon. Log-log scale plot.

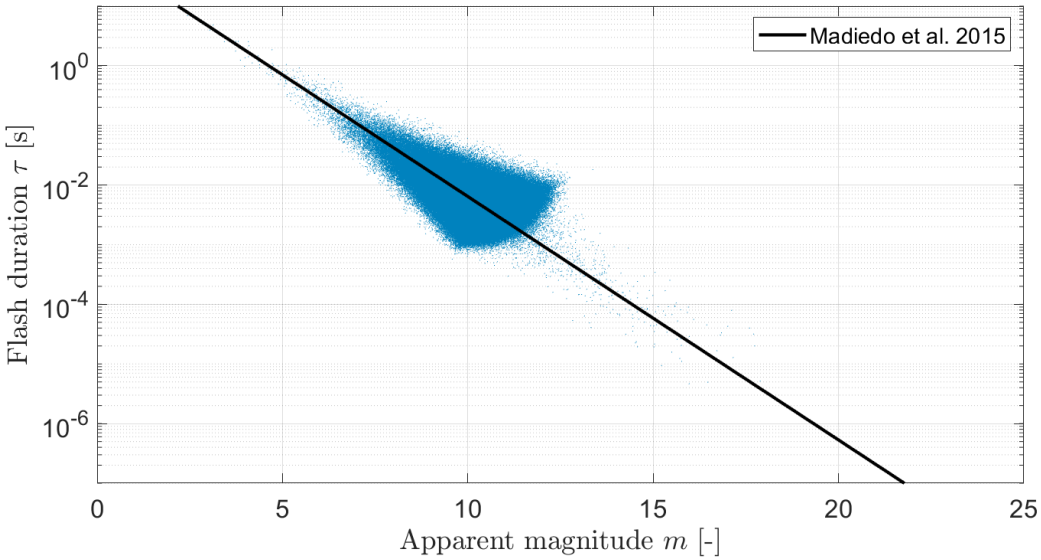

Figure 21: Apparent magnitude and flash duration correlation of lunar impacts (2024 scenario). The blue dots are the outputs of MeGun. The solid black line is the empirical correlation provided in [6]. KE $\geq 10^{-7}$ kton TNT Equivalent, Moon equivalent. Semi-log scale plot.

solid line is the empirical law in [36], see Equation (10). In addition, there are two horizontal dashed red lines that represent the range of luminous efficiencies reported in the literature from observations of major streams [5, 51, 56]. Also in this case, simulation results and the black solid line are in such agreement as a consequence of the underlying model (see Section 3.3).

Eventually, Figure 23 shows the equivalent black body temperature computed as a function of the impact kinetic energy at the Moon. In the chart, the horizontal dashed black line represents the reference temperature indicated in [5]. There are also two horizontal dashed red lines highlighting the range of temperature measurements reported in the literature [55]. Results are slightly smaller than real measurements. The reason may be that in our method an average equivalent black body temperature is computed (see Equation (21)), while measurements refer to the peak one, corresponding to the magnitude peak of the impact flash.

6.3.4 Synthesis of impact dynamics

A synthesis of the analysis conducted is hereafter carried out. A scenario like the sample one (during year 2024) counts almost 2 million impacts (precisely, 1 750 823). Therefore, the data population is large enough to infer good statistical results. All samples have impact kinetic energies greater than or equal to 10^{-7} kton TNT Equivalent at the Moon. However, the focus of this analysis is on the impacts that fall in the range of impact kinetic energies $[10^{-6}, 10^{-1}]$ kton TNT Equivalent at the Earth (corresponding to $[7.33 \times 10^{-7}, 7.33 \times 10^{-2}]$ kton TNT Equivalent at the Moon), which

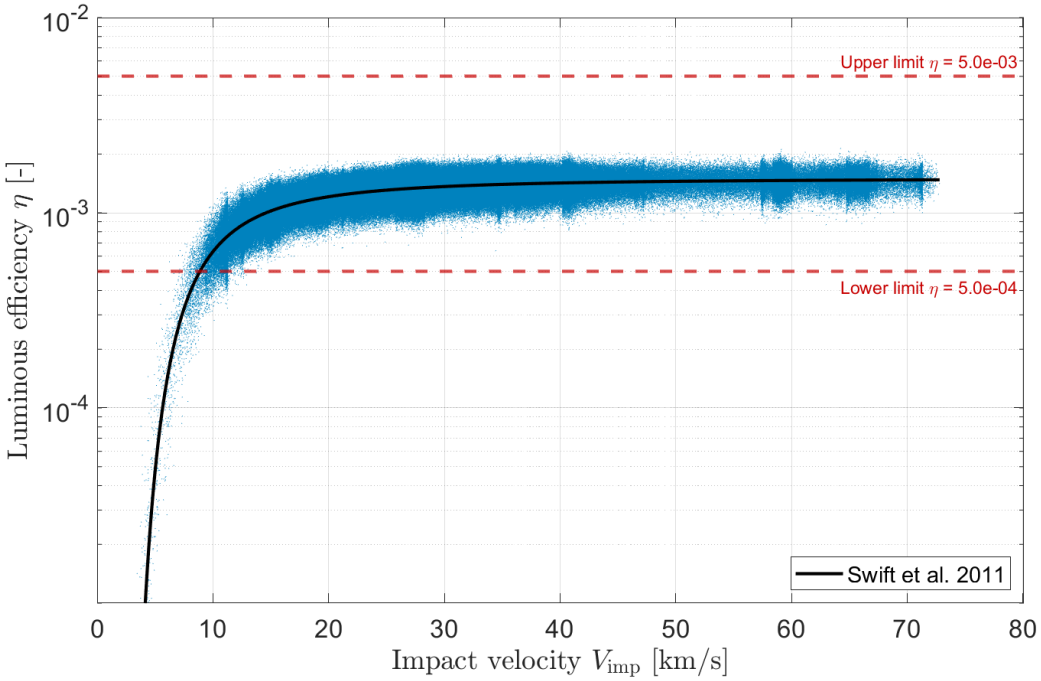

Figure 22: Luminous efficiencies of lunar impacts (2024 scenario). The luminous efficiency is represented by tiny blue dots and is plotted versus the impact velocity. The solid black line is the empirical correlation provided by [36]. The two horizontal dashed red lines mark the range of luminous efficiencies reported in the literature [5, 51, 56]. KE $\geq 10^{-7}$ kton TNT Equivalent, Moon equivalent. Semi-log scale plot.

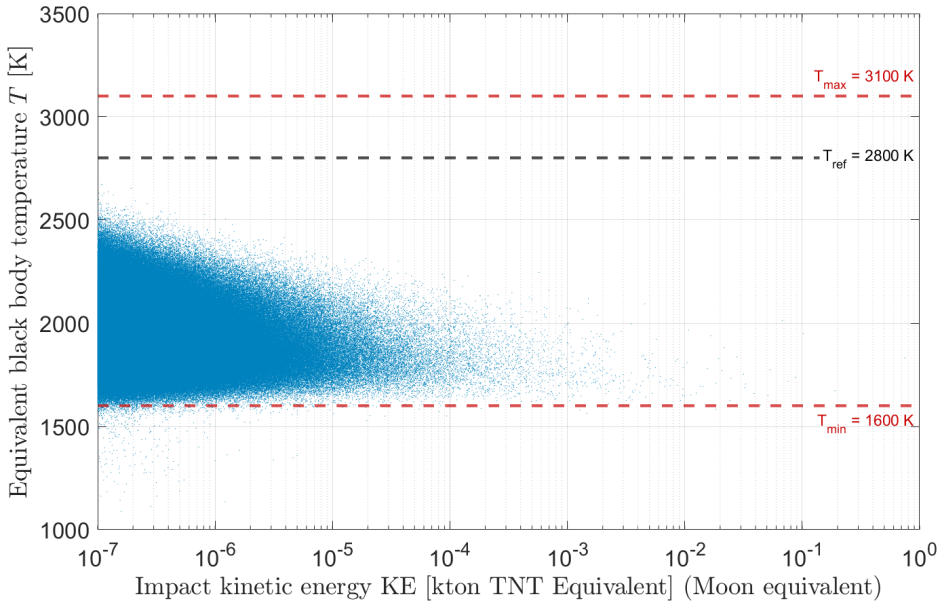

Figure 23: Radiating plume equivalent black body temperatures of lunar impacts (2024 scenario). Temperature as a function of impact kinetic energy at the Moon is represented by the blue dots. The horizontal dashed black line shows the reference value suggested in [5]. Differently, the two horizontal dashed red lines mark the range of temperature measurements reported in [55]. Semi-log scale plot.

Table 5: Statistics about impact dynamics.

Quantity			Value
	$\mathcal{N}_{\text{pool}}$	[#]	217 947
Black body temperature	μ_T	[K]	1900
	σ_T	[K]	130
	$\pm 3\sigma_T$ Range	[K]	[1510, 2290]
	T_{min}	[K]	1130
	T_{max}	[K]	2530
Flash duration	μ_τ	[ms]	15
	σ_τ	[ms]	25
	$\pm 3\sigma_\tau$ Range	[ms]	(0, 90]
	τ_{min}	[ms]	6×10^{-2}
	τ_{max}	[s]	2.6
Plume area	μ_{Ap}	[m^2]	70
	σ_{Ap}	[m^2]	220
	$\pm 3\sigma_{Ap}$ Range	[m^2]	(0, 730]
	$A_{p,\text{min}}$	[m^2]	4
	$A_{p,\text{max}}$	[m^2]	35 270

is the one of interest for the LUMIO mission.

Considering the sample scenario, there are 217 947 meteoroids with impact kinetic energy within the range of interest. The pool is still large enough to obtain meaningful statistical results. The results in terms of means and standard deviations of equivalent black body temperature of the flash, impact flash duration, and plume areas are shown in Table 5.

Equivalent black body temperature ranges between 1510 K and 2290 K, $\pm 3\sigma_T$ range. The range is consistent with the temperatures measured within the NELIOTA project (1600–3100 K as reported in [55] and 1300–5800 K as subsequently detailed in [63]). The temperature range $[1700, 3800]$ K suggested in [60] is coherent with the results, although the maximum temperature returned by our method is lower. The mean is slightly lower than the reference values proposed by [5], but it should be considered that in the presented methodology the average temperature is computed, and not the peak one.

According to [56], impact flash duration ranges from $\approx$ 10 ms to $\approx$ 1 s. The NELIOTA programme reports durations between 33 ms and 165 ms, where the lower bound is the exposure time of the cameras. Similarly, flashes that last from 20 ms to 160 ms are reported in [6]. In [20], a value of 10 ms is used to perform the LUMIO mission orbit design. Values greater than 0 ms and up to 90 ms are found considering the truncated $\pm 3\sigma_\tau$ range limited to positive values. Results have the same order of magnitude of the ones reported in the literature. Nevertheless, the average duration

of 15 ms is slightly smaller than the typical values reported in the literature while it is in line with the value employed in [20].

The plume areas span from values greater than $0\,\mathrm{m}^2$ and up to $730\,\mathrm{m}^2$, truncated $\pm 3\sigma_{Ap}$ range. Range has been truncated to keep only positives values.

7 Conclusion

In this work, a comprehensive stochastic model of the lunar meteoroid environment that unifies methods, experimental observations, and empirical laws has been presented. Known meteor showers and the sporadic background have been collected in the form of a catalog. The methodology has been devised to support the design and estimate the scientific return of the LUMIO lunar CubeSat mission. Sample scenarios have been reproduced to compare meteoroid fluxes computed with our method against available power laws. Results show good agreement between our model and the meteoroid fluxes reported in the literature. As an example, the energy distribution of impacts and the estimation of LUMIO's scientific return have been presented, together with the details of a sample scenario of the year 2024.

Under the assumptions discussed, the proposed novel methodology could be applied in different space-related applications other than the LUMIO mission. For instance, scenarios of the meteoroid environment can be used to statistically determine the energetic, spatial, and temporal distributions of meteoroids colliding with a spacecraft. Additionally, safe spots for future lunar settlements can be localized. Again, foreseeing meteoroid fluxes, the schedule of observation windows from Earth-based assets can be optimized if an atmosphere and an entry dynamics model to simulate effectively fireballs and meteor showers phenomena are implemented. As a consequence, the envisaged procedural generation for meteoroid impacts may prove useful for the relevant community, therefore we make the implemented tool MeGun available to interested community.

Acknowledgments

Part of this work has been conducted under ESA Contract No. 4000130257/20/NL/AS within the GSTP, and has received support from the national delegations of Italy (ASI), the Netherlands (NSO), and Norway (NOSA). The authors would like to acknowledge the members of the LUMIO team for their support and the ESA experts for reviewing the Phases 0 and A design. The authors would like to thank Dr. D. Koschny, Scientist in ESA's Planetary Defence Office, for the constructive feedback provided about the meteoroid environment modeling. The authors would like to thank the anonymous reviewers for the helpful comments at the review stage.

A Catalog

The lists of established meteor showers and the ones used to generate meteoroid streams in our model are presented in Table 6. The catalog of showers is shown in Table 7. If a quantity is missing, it means the values was not found in the literature. In that case, the quantity is assumed according to the following indications:

- if the mean of population index χ is missing, $\mu_\chi = 2.5$ is assumed;
- if the mean of ZHR is missing, $\mu_{\mathrm{ZHR}} = 1\,\mathrm{h}^{-1}$ is assumed;
- if the mean of full-width-half-maximum W is missing, $\mu_W = 2$ is assumed;
- if information of meteoroid bulk density ρ is missing, a bi-modal distribution is used to describe rocky or iron objects. For rocky objects the mean value $1800\,\mathrm{kg\,m}^{-3}$ and a standard deviation equal to $300\,\mathrm{kg\,m}^{-3}$ is used [25]. For iron objects the mean used is $7370\,\mathrm{kg\,m}^{-3}$ [55], with a standard deviation equal to the 10% of the mean. The draws of the bi-modal distribution are limited between $[1500, 7874]$ $\mathrm{kg\,m}^{-3}$. The upper bound is the iron density;
- if the standard deviation of radiant RA or DEC is missing, $\sigma_{\mathrm{RA,DEC}} = 5\,\mathrm{deg}$ is assumed;
- in general, if the standard deviation of a quantity is missing, $\sigma_x = 0.1\mu_x$ is assumed, except if otherwise specified (see previous indications).

The shower catalog has been built collecting information from the catalogs included in [12–14, 25–29]. The catalog of the sporadic background sources can be found in Table 8. Data have been taken from [30].

Table 6: List of established meteor showers. The first column contains the IDs of meteor showers, while in the second column there is the IAU code. The third column contains the extended name. Then, the fourth column, named "Gen.", informs if the shower is used to generate a stream by MeGun (green tick) or not (red X). If it is not generated a brief motivation is provided in the last column. In the list there are 112 meteor showers, which are all the showers currently in the Established List provided by MDC.

#ID	IAU Code	Extended Name	Gen.	Notes
#1	CAP	α-Capricornids	✓	-
#2	STA	Southern Taurids	✓	-
#4	GEM	Geminids	✓	-
#5	SDA	Southern δ-Aquariids	✓	-
#6	LYR	April Lyrids	✓	-
#7	PER	Perseids	✓	-
#8	ORI	Orionids	✓	-
#9	DRA	October Draconids	✓	-
#10	QUA	Quadrantids	✓	-
#11	EVI	η-Virginids	✓	-
#12	KCG	κ-Cygnids	✓	-
#13	LEO	Leonids	✓	-
#15	URS	Ursids	✓	-
#16	HYD	σ-Hydrids	✓	-
#17	NTA	Northern Taurids	✓	-
#18	AND	Andromedids	X	Lack of Data
#19	MON	December Monocerotids	✓	-
#20	COM	Comae Berenicids	✓	-
#21	AVB	α-Virginids	✓	-
#22	LMI	Leonis Minorids	✓	-
#23	EGE	ε-Geminids	✓	-
#26	NDA	Northern δ-Acquariids	✓	-
#27	KSE	κ-Serpentids	✓	-
#31	ETA	η-Aquariids	✓	-
#33	NIA	Northern ι-Acquariids	✓	-
#61	TAH	τ-Herculids	✓	-
#63	COR	Corvids	X	Lack of Data
#69	SSG	Southern μ-Sagittariids	✓	-
#96	NCC	Northern δ-Cancrids	✓	-
#97	SCC	Southern δ-Cancrids	✓	-
#100	XSA	Daytime ξ-Sagittariids	X	Lack of Data
#102	ACE	α-Centaurids	✓	-
#110	AAN	α-Antliids	✓	-
#128	MKA	Daytime κ-Aquariids	X	Lack of Data
#137	PPU	π-Puppids	✓	-
#144	APS	Daytime April Piscids	X	Lack of Data
#145	ELY	η-Lyrids	✓	-
#151	EAU	ε-Aquilids	X	Lack of Data
#152	NOC	Northern Daytime ω-Cetids	✓	-
#153	OCE	southern Daytime ω-Cetids	✓	-

Table 6: List of established meteor showers (cont'd).

#ID	IAU Code	Extended Name	Gen.	Notes
#156	SMA	Southern Daytime May Arietids	✓	-
#164	NZC	Northern June Aquilids	✓	-
#165	SZC	Southern June Aquilids	✓	-
#170	JBO	June Bootids	✓	-
#171	ARI	Daytime Arietids	✓	-
#172	ZPE	Daytime ζ-Perseids	✓	-
#173	BTA	Daytime β-Taurids	✓	-
#175	JPE	July Pegasids	✓	-
#183	PAU	Piscis Austrinids	✓	-
#184	GDR	July γ-Draconids	X	Lack of Data
#187	PCA	ψ-Cassiopeiids	X	Lack of Data
#188	XRI	Daytime ξ-Orionids	X	Lack of Data
#191	ERI	η-Eridanids	✓	-
#197	AUD	August Draconids	X	Lack of Data
#198	BHY	β-Hydrusids	X	Lack of Data
#202	ZCA	Daytime ζ-Cancrids	X	Lack of Data
#206	AUR	Aurigids	✓	-
#208	SPE	September ε-Perseids	X	Lack of Data
#212	KLE	Daytime κ-Leonids	X	Lack of Data
#221	DSX	Daytime Sextantids	✓	-
#233	OCC	October Capricornids	✓	-
#242	XDR	ξ-Draconids	X	Lack of Data
#246	AMO	α-Monocerotids	✓	-
#250	NOO	November Orionids	X	Lack of Data
#252	ALY	α-Lyncids	X	Lack of Data
#254	PHO	Phoenicids	✓	-
#257	ORS	Southern χ-Orionids	✓	-
#281	OCT	October Camelopardalids	X	Lack of Data
#319	JLE	January Leonids	X	Lack of Data
#320	OSE	ω-Serpentids	X	Lack of Data
#321	TCB	θ-Coronae Borealids	X	Lack of Data
#322	LBO	λ-Bootids	X	Lack of Data
#323	XCB	ξ-Coronae Borealids	X	Lack of Data
#324	EPR	ε-Perseids	X	Lack of Data
#325	DLT	Daytime λ-Taurids	X	Lack of Data
#326	EPG	ε-Pegasids	X	Lack of Data
#327	BEQ	β-Equuleids	X	Lack of Data
#328	ALA	α-Lacertids	X	Lack of Data
#330	SSE	σ-Serpentids	X	Lack of Data
#331	AHY	α-Hydrids	X	Lack of Data
#333	OCU	October Ursae Majorids	X	Lack of Data
#334	DAD	December α-Draconids	X	Lack of Data
#335	XVI	December χ-Virginids	X	Lack of Data
#336	DKD	December κ-Draconids	X	Lack of Data

Table 6: List of established meteor showers (cont'd).

#ID	IAU Code	Extended Name	Gen.	Notes
#337	NUE	ν-Eridanids	X	Lack of Data
#338	OER	o-Eridanids	X	Lack of Data
#339	PSU	ψ-Ursae Majorids	X	Lack of Data
#341	XUM	January ξ-Ursae Majorids	X	Lack of Data
#343	HVI	h-Virginids	X	Lack of Data
#346	XHE	x-Herculids	X	Lack of Data
#348	ARC	April ρ-Cygnids	X	Lack of Data
#362	JMC	June μ-Cassiopeiids	X	Lack of Data
#372	PPS	ϕ-Piscids	X	Lack of Data
#388	CTA	χ-Taurids	X	Lack of Data
#390	THA	November θ-Aurigids	X	Lack of Data
#404	GUM	γ-Ursae Minorids	X	Lack of Data
#411	CAN	c-Andromedids	X	Lack of Data
#427	FED	February η-Draconids	X	Lack of Data
#428	DSV	December σ-Virginids	X	Lack of Data
#431	JIP	June ι-Pegasids	X	Lack of Data
#445	KUM	κ-Ursae Majorids	X	Lack of Data
#446	DPC	December ϕ-Cassiopeiids	X	Lack of Data
#506	FEV	February ε-Virginids	X	Lack of Data
#510	JRC	June ρ-Cygnids	X	Lack of Data
#512	RPU	ρ-Puppids	X	Lack of Data
#524	LUM	λ-Ursae Majorids	X	Lack of Data
#526	SLD	Southern λ-Draconids	X	Lack of Data
#529	EHY	η-Hydrids	X	Lack of Data
#530	ECV	η-Corvids	X	Lack of Data
#533	JXA	July ξ-Arietids	X	Lack of Data
#549	FAN	Andromedids	X	Lack of Data
#569	OHY	o-Hydrids	X	Lack of Data

Table 7: Catalog of meteor showers from MDC's Established List. In the first column there is the ID of the shower. Next, there is its the activity period. Start, peak, and end of activity period are expressed in terms of solar longitudes. Then, information about radiant direction and drift are provided. RA and DEC of radiant at the activity peak of shower are expressed with mean and standard deviation. Data about radiant drift are also included and expressed in degrees per unit degree of solar longitude. In columns eleven and twelve, there are geocentric velocity mean and standard deviation. Thirteenth and fourteenth columns contain mean and standard deviation of ZHR at epoch of activity peak, respectively. The next two columns present mean and standard deviation of full-width-half-maximum parameter W. It follows the population index χ. The last two columns are reserved to bulk density mean and standard deviation. When a quantity is missing, the symbol '-' is used. The meteor shower catalog has been built merging information from catalogs included in [12–14, 25–29].

#ID	$\lambda_\odot$ [deg]			RA [deg]		DEC [deg]		$\frac{\Delta RA}{\Delta\lambda_\odot}$ [deg/deg]	$\frac{\Delta DEC}{\Delta\lambda_\odot}$ [deg/deg]	V [km s^{-1}]		ZHR [h^{-1}]		W [deg]		χ [–]	ρ [kg m^{-3}]	
	Start	Peak	End	μ_{RA}	σ_{RA}	μ_{DEC}	σ_{DEC}			μ_V	σ_V	μ_{ZHR}	σ_{ZHR}	μ_W	σ_W		μ_ρ	σ_ρ
#1	101.0	127.0	138.0	+306.5	2.2	-9.2	1.0	+0.97	+0.24	23.0	1.2	2.0	-	15.10	2.60	2.20	2100	-
#2	180.0	216.0	272.0	+47.9	5.8	+12.8	3.0	+0.99	+0.26	26.6	3.5	3.3	-	22.00	3.00	2.30	-	-
#4	243.0	262.0	270.0	+113.5	2.8	+32.3	1.5	+1.15	-0.16	33.8	2.0	120.0	10.0	0.90	0.10	2.00	2900	600
#5	117.0	128.0	146.0	+341.3	1.9	-15.7	1.1	+0.95	+0.38	41.3	3.0	18.0	4.0	13.00	2.00	3.30	-	-
#6	21.0	32.0	45.0	+272.0	2.1	+33.4	1.5	+0.66	+0.02	46.7	1.5	12.8	0.7	2.74	0.13	2.90	-	-
#7	115.0	140.0	158.0	+48.2	2.8	+58.1	1.7	+1.40	+0.26	59.1	2.4	84.0	5.0	3.01	0.16	2.50	-	-
#8	180.0	209.0	245.0	+95.9	2.6	+15.7	1.4	+1.03	-0.05	66.3	2.1	23.0	4.0	5.40	0.60	2.90	-	-
#9	195.0	195.0	196.0	+262.9	1.4	+55.7	0.9	+0.34	-0.05	20.7	3.6	1.0	-	-	-	2.60	-	-
#10	270.0	283.0	297.0	+230.2	3.3	+49.5	2.4	+0.56	-0.25	40.7	2.2	130.0	24.0	0.35	0.05	2.20	1900	200
#11	343.0	357.0	359.0	+184.8	8.0	+3.9	2.5	+0.92	-0.40	26.6	3.3	1.5	-	8.00	-	3.00	-	-
#12	136.0	141.0	144.0	+277.5	3.1	+52.8	2.9	+0.40	+0.05	20.9	0.7	2.3	0.4	8.80	0.70	2.20	2200	1700
#13	220.0	235.0	248.0	+153.8	1.6	+21.8	0.7	+0.99	-0.36	70.2	1.8	13.0	3.0	3.00	0.60	2.50	-	-
#15	267.0	271.0	271.0	+219.9	3.2	+75.4	1.1	+0.05	-0.31	32.9	0.8	12.0	3.0	0.70	-	3.40	-	-
#16	188.0	266.0	275.0	+134.4	5.9	-0.1	1.2	+0.92	-0.28	58.9	2.3	2.5	0.5	6.60	2.00	3.00	-	-
#17	181.0	220.0	267.0	+48.9	5.2	+20.7	1.6	+1.03	+0.26	28.0	3.1	4.0	-	22.00	3.00	2.30	-	-
#18	213.0	223.0	235.0	+20.7	4.8	+28.0	1.7	+1.00	+0.37	18.2	1.1	-	-	18.00	-	-	-	-
#19	246.0	261.0	275.0	+102.9	1.9	+7.8	1.3	+0.97	-0.09	41.4	2.2	2.0	0.4	4.00	3.00	3.00	-	-
#20	252.0	274.0	302.0	+167.0	1.6	+28.0	0.9	+0.96	-0.39	63.3	1.6	3.2	0.7	26.00	-	3.00	-	-
#21	25.0	32.0	37.0	+203.5	1.4	+2.9	2.1	+0.91	-0.36	18.8	0.8	5.0	-	8.60	-	-	-	-
#22	199.0	209.0	223.0	+159.9	1.1	+36.6	1.0	+1.02	-0.38	61.9	1.3	1.9	0.7	4.30	1.20	2.70	-	-

Table 7: Catalog of meteor showers from MDC's Established List (cont'd).

#ID	$\lambda_\odot$ [deg]			RA [deg]		DEC [deg]		$\frac{\Delta RA}{\Delta\lambda_\odot}$ [deg/deg]	$\frac{\Delta DEC}{\Delta\lambda_\odot}$ [deg/deg]	V [km s^{-1}]		ZHR [h^{-1}]		W [deg]		χ [–]	ρ [kg m^{-3}]	
	Start	Peak	End	μ_{RA}	σ_{RA}	μ_{DEC}	σ_{DEC}			μ_V	σ_V	μ_{ZHR}	σ_{ZHR}	μ_W	σ_W		μ_ρ	σ_ρ
#23	187.0	198.0	212.0	+93.8	2.1	+28.1	1.3	+1.13	-0.03	69.6	0.8	1.6	-	15.00	-	3.00	-	-
#26	120.0	141.0	154.0	+347.6	6.7	+2.1	2.3	+0.91	+0.39	38.4	3.1	1.0	0.2	11.80	2.30	3.30	-	-
#27	3.0	20.0	27.0	+240.2	3.5	+16.8	2.1	+0.81	-0.20	46.7	2.9	4.0	-	3.00	-	-	-	-
#31	27.0	46.0	64.0	+338.1	1.5	-0.8	0.9	+0.92	+0.37	65.7	2.0	28.0	4.0	11.00	0.70	2.70	-	-
#33	133.0	148.0	160.0	+346.7	2.7	-1.2	2.2	+0.92	+0.39	31.3	3.1	2.1	-	33.00	-	3.20	-	-
#61	58.0	72.0	83.0	+228.5	-	+39.8	-	+0.90	-0.10	15.0	-	2.0	-	11.00	-	-	-	-
#63	79.0	86.0	95.0	+205.8	8.4	+0.2	11.6	+0.92	-0.36	8.7	0.5	-	-	-	-	-	-	-
#69	77.0	86.0	104.0	+273.2	3.0	-29.5	1.5	+1.14	+0.03	25.1	1.6	1.5	-	12.00	-	2.80	-	-
#96	273.0	296.0	303.0	+127.6	3.3	+21.5	1.6	+1.04	-0.25	27.2	1.9	1.6	-	10.00	-	3.00	-	-
#97	278.0	296.0	298.0	+125.0	3.2	+14.4	1.7	+1.00	-0.23	27.0	1.8	1.6	-	10.00	-	3.00	-	-
#100	296.0	304.9	311.0	+283.2	-	-21.9	-	+0.00	+0.00	24.4	-	-	-	-	-	-	-	-
#102	312.0	319.4	330.0	+210.9	-	-58.2	-	+1.90	-0.50	58.2	-	7.3	1.5	3.40	0.60	2.00	-	-
#110	304.0	312.0	328.0	+157.2	2.5	-9.5	1.7	+0.89	-0.37	45.0	2.6	2.0	-	1.60	-	3.40	-	-
#128	352.0	354.0	356.0	+338.7	-	-7.7	-	+0.00	+0.00	33.2	-	-	-	-	-	-	-	-
#137	25.0	33.6	38.0	+110.4	-	-45.1	-	+0.40	-0.10	15.0	-	1.0	-	5.00	-	2.00	-	-
#144	16.0	26.0	38.0	+4.9	-	+5.5	-	+0.94	+0.42	29.2	-	-	-	8.00	-	-	-	-
#145	47.0	49.0	53.0	+289.9	1.6	+43.4	1.0	+0.56	+0.14	43.7	0.8	3.0	1.0	2.00	-	-	-	-
#151	58.0	63.0	73.0	+294.1	3.8	+20.4	2.5	+0.78	+0.17	31.5	1.7	-	-	5.00	-	-	-	-
#152	16.0	49.0	61.0	+11.8	-	+18.9	-	+0.99	+0.36	36.2	-	2.0	-	12.00	-	-	-	-
#153	11.0	49.0	65.0	+23.4	-	-4.3	-	+0.91	+0.46	37.0	-	8.0	-	12.00	2.00	-	-	-
#156	36.0	54.0	59.0	+36.3	-	+10.8	-	+0.96	+0.30	28.0	-	2.0	-	-	-	-	-	-
#164	75.0	101.0	119.0	+309.7	2.4	-5.3	2.5	+0.95	+0.26	38.3	2.9	3.0	-	9.00	-	-	-	-
#165	79.0	104.0	115.0	+319.3	4.0	-27.6	2.1	+1.05	+0.30	39.2	2.7	1.4	-	9.00	-	-	-	-
#170	95.0	96.3	99.0	+219.0	-	+49.0	-	+0.60	-0.40	13.9	-	1.0	-	1.60	-	-	-	-
#171	73.0	77.0	90.0	+43.9	1.3	+24.4	1.2	+1.05	+0.28	41.1	1.6	54.0	12.0	6.60	2.00	2.70	-	-

Table 7: Catalog of meteor showers from MDC's Established List (cont'd).

#ID	$\lambda_\odot$ [deg]			RA [deg]		DEC [deg]		$\frac{\Delta RA}{\Delta\lambda_\odot}$ [deg/deg]	$\frac{\Delta DEC}{\Delta\lambda_\odot}$ [deg/deg]	V [km s^{-1}]		ZHR [h^{-1}]		W [deg]		χ [–]	ρ [kg m^{-3}]	
	Start	Peak	End	μ_{RA}	σ_{RA}	μ_{DEC}	σ_{DEC}			μ_V	σ_V	μ_{ZHR}	σ_{ZHR}	μ_W	σ_W		μ_ρ	σ_ρ
#172	56.0	74.0	90.0	+56.6	-	+23.2	-	+0.99	+0.23	27.1	-	20.0	-	18.00	-	2.70	-	-
#173	89.0	94.0	101.0	+82.8	-	+20.1	-	+0.82	+0.05	26.8	-	10.0	-	17.00	-	-	-	-
#175	98.0	108.0	143.0	+347.2	1.5	+10.0	1.9	+0.90	+0.39	64.0	1.3	2.7	-	3.50	-	3.00	-	-
#183	125.0	136.0	146.0	+352.5	1.7	-20.5	1.3	+0.94	+0.40	43.8	1.1	2.9	0.8	2.40	0.50	3.20	-	-
#184	119.0	124.0	127.0	+280.1	2.0	+50.3	0.9	+0.45	+0.07	27.5	0.9	-	-	3.20	-	-	-	-
#187	103.0	119.0	135.0	+36.8	17.6	+72.2	3.2	+1.68	+0.32	42.0	2.5	-	-	2.00	-	-	-	-
#188	128.0	137.0	140.0	+107.5	-	+16.2	-	+0.70	-0.10	43.8	-	-	-	-	-	-	-	-
#191	118.0	137.0	174.0	+43.7	1.7	-11.9	2.3	+0.86	+0.29	64.5	2.4	6.0	-	4.00	-	-	-	-
#197	140.0	143.0	146.0	+271.7	2.3	+58.9	0.6	+0.26	+0.01	21.1	0.6	-	-	3.00	-	-	-	-
#198	143.0	143.8	144.0	+33.2	-	-75.1	-	+0.00	+0.00	27.0	-	-	-	-	-	-	-	-
#202	140.0	160.0	167.0	+136.1	-	+11.7	-	+0.92	-0.18	42.1	-	-	-	-	-	-	-	-
#206	145.0	158.0	164.0	+90.9	1.5	+38.6	1.3	+1.24	-0.01	65.6	1.1	4.0	1.0	2.70	-	2.60	-	-
#208	161.0	168.0	190.0	+48.6	1.2	+39.6	1.4	+1.17	+0.26	64.8	1.0	-	-	6.00	-	-	-	-
#212	164.0	183.0	200.0	+162.3	-	+14.9	-	+0.62	-0.30	43.3	-	-	-	3.00	-	-	-	-
#221	179.0	188.0	191.0	+156.6	2.1	-2.4	0.8	+0.91	-0.37	32.9	1.1	20.0	-	2.00	0.20	-	-	-
#233	177.0	189.7	211.0	+303.0	-	-10.0	-	+0.90	+0.20	10.0	-	2.3	1.5	-	-	-	-	-
#242	209.0	211.0	215.0	+171.2	-	+70.6	-	+0.98	-0.63	37.1	-	-	-	12.00	-	-	-	-
#246	238.0	239.0	240.0	+90.9	0.1	+38.6	0.2	+0.97	-0.09	65.6	0.2	3.5	-	3.80	-	2.70	-	-
#250	225.0	247.0	265.0	+90.6	2.6	+15.2	1.4	+1.03	-0.01	42.5	2.5	-	-	5.00	-	-	-	-
#252	266.0	272.0	274.0	+140.4	0.4	+39.8	0.2	+1.13	-0.31	49.5	1.5	-	-	-	-	-	-	-
#254	252.0	253.0	254.0	+15.6	-	-44.7	-	+0.00	+0.00	11.7	-	3.0	-	2.80	1.50	2.90	-	-
#257	238.0	243.0	268.0	+73.0	1.6	+17.8	1.2	+1.04	+0.11	27.9	1.4	0.6	-	22.00	-	-	-	-
#281	190.0	193.0	194.0	+166.0	-	+79.1	-	+0.00	+0.00	46.6	-	-	-	-	-	-	-	-
#319	279.0	283.0	287.0	+147.7	1.4	+24.1	0.5	+1.01	-0.34	51.4	0.9	-	-	-	-	-	-	-
#320	277.0	280.5	281.0	+157.3	0.1	+27.3	1.0	+0.99	-0.37	45.0	0.2	-	-	-	-	-	-	-

Table 7: Catalog of meteor showers from MDC's Established List (cont'd).

#ID	$\lambda_\odot$ [deg]			RA [deg]		DEC [deg]		$\frac{\Delta RA}{\Delta\lambda_\odot}$ [deg/deg]	$\frac{\Delta DEC}{\Delta\lambda_\odot}$ [deg/deg]	V [km s^{-1}]		ZHR [h^{-1}]		W [deg]		χ [–]	ρ [kg m^{-3}]	
	Start	Peak	End	μ_{RA}	σ_{RA}	μ_{DEC}	σ_{DEC}			μ_V	σ_V	μ_{ZHR}	σ_{ZHR}	μ_W	σ_W		μ_ρ	σ_ρ
#321	287.0	296.0	304.0	+233.6	-	+34.4	-	+0.30	+0.16	37.7	-	-	-	-	-	-	-	-
#322	280.0	296.0	297.0	+221.5	-	+42.4	-	+1.04	-0.76	40.7	-	-	-	-	-	-	-	-
#323	293.0	296.0	300.0	+250.9	2.2	+29.7	1.3	+0.70	-0.13	45.1	1.4	-	-	-	-	-	-	-
#324	86.0	88.0	91.0	+53.8	0.9	+37.8	0.4	+1.17	+0.23	43.8	0.7	-	-	-	-	-	-	-
#325	71.0	86.0	98.0	+57.3	-	+11.4	-	+0.85	+0.33	35.6	-	-	-	-	-	-	-	-
#326	101.0	109.0	120.0	+330.2	7.0	+13.0	5.6	+0.87	+0.35	28.4	2.7	-	-	-	-	-	-	-
#327	77.0	91.0	98.0	+305.1	2.9	+1.1	2.4	+0.91	+0.23	33.2	2.1	-	-	-	-	-	-	-
#328	108.0	109.0	121.0	+349.4	2.3	+54.4	0.2	+0.82	+0.39	37.4	0.3	-	-	-	-	-	-	-
#330	272.0	276.0	291.0	+245.4	1.0	-4.8	1.0	+0.95	-0.16	45.5	0.2	-	-	-	-	-	-	-
#331	265.0	284.0	297.0	+126.9	2.2	-8.7	2.1	+0.87	-0.24	43.3	2.3	-	-	-	-	-	-	-
#333	201.0	202.0	203.0	+145.0	1.6	+64.8	0.7	+1.39	-0.33	55.6	1.3	-	-	-	-	-	-	-
#334	248.0	256.0	263.0	+210.8	5.1	+58.6	2.7	+0.58	-0.34	40.8	1.5	-	-	-	-	-	-	-
#335	248.0	267.0	280.0	+194.3	2.1	-12.0	1.0	+0.94	-0.39	69.1	2.0	-	-	-	-	-	-	-
#336	250.0	252.0	255.0	+187.2	2.7	+70.2	1.3	+0.77	-0.39	43.8	1.0	-	-	-	-	-	-	-
#337	150.0	163.0	234.0	+61.5	3.1	+4.3	4.2	+0.95	+0.19	67.1	2.4	-	-	-	-	-	-	-
#338	216.0	232.0	242.0	+59.9	2.4	+0.1	2.9	+0.92	+0.20	28.5	2.0	-	-	-	-	-	-	-
#339	250.0	253.0	258.0	+169.8	1.2	+42.4	1.1	+0.98	-0.39	61.7	0.7	-	-	-	-	-	-	-
#341	295.0	298.0	302.0	+168.7	2.2	+33.0	1.0	+0.97	-0.39	40.9	2.3	-	-	-	-	-	-	-
#343	38.0	38.0	44.0	+204.8	2.0	-11.5	2.1	+0.95	-0.36	17.2	0.8	-	-	-	-	-	-	-
#346	348.0	350.0	352.0	+253.0	0.9	+49.2	0.5	+0.48	-0.10	35.2	1.2	-	-	-	-	-	-	-
#348	36.0	38.0	44.0	+322.1	3.2	+46.6	2.1	+0.66	+0.32	40.9	1.7	-	-	-	-	-	-	-
#362	58.0	77.0	84.0	+15.8	5.6	+55.4	2.3	+1.08	+0.38	41.7	2.4	-	-	-	-	-	-	-
#372	78.0	103.0	130.0	+17.0	2.5	+25.0	2.4	+0.97	+0.38	66.5	1.6	-	-	-	-	-	-	-
#388	207.0	221.0	235.0	+63.0	2.1	+26.2	1.5	+1.09	+0.18	41.1	2.6	-	-	-	-	-	-	-
#390	229.0	244.0	249.0	+95.7	4.1	+34.7	2.5	+1.19	-0.04	32.5	3.7	-	-	-	-	-	-	-

Table 7: Catalog of meteor showers from MDC's Established List (cont'd).

#ID	$\lambda_\odot$ [deg]			RA [deg]		DEC [deg]		$\frac{\Delta RA}{\Delta\lambda_\odot}$ [deg/deg]	$\frac{\Delta DEC}{\Delta\lambda_\odot}$ [deg/deg]	V [km s^{-1}]		ZHR [h^{-1}]		W [deg]		χ [–]	ρ [kg m^{-3}]	
	Start	Peak	End	μ_{RA}	σ_{RA}	μ_{DEC}	σ_{DEC}			μ_V	σ_V	μ_{ZHR}	σ_{ZHR}	μ_W	σ_W		μ_ρ	σ_ρ
#404	289.0	298.0	300.0	+228.3	5.6	+69.2	1.9	+0.14	-0.26	28.8	1.2	-	-	-	-	-	-	-
#411	94.0	107.0	124.0	+29.1	2.4	+47.3	1.8	+1.13	+0.35	57.5	1.4	-	-	-	-	-	-	-
#427	314.0	315.0	316.0	+239.6	0.8	+62.4	0.6	+0.26	-0.20	35.1	0.9	-	-	-	-	-	-	-
#428	249.0	262.0	271.0	+200.8	0.7	+5.8	0.8	+0.90	-0.37	66.2	1.7	-	-	-	-	-	-	-
#431	91.0	94.0	96.0	+332.1	2.0	+29.1	0.5	+0.81	+0.35	58.5	1.0	-	-	-	-	-	-	-
#445	221.0	225.0	228.0	+147.2	0.4	+45.0	0.9	+1.13	-0.34	65.7	0.8	-	-	-	-	-	-	-
#446	246.0	252.0	258.0	+19.5	3.2	+57.7	1.5	+1.14	+0.37	16.5	1.1	-	-	-	-	-	-	-
#506	300.0	314.0	328.0	+200.4	1.8	+11.0	1.3	+0.89	-0.37	62.9	1.4	-	-	-	-	-	-	-
#510	82.0	84.0	87.0	+320.5	1.9	+44.1	0.7	+0.67	+0.31	50.9	1.0	-	-	-	-	-	-	-
#512	226.0	231.0	237.0	+130.4	2.6	-26.3	1.5	+0.77	-0.26	57.8	2.9	-	-	-	-	-	-	-
#524	213.0	214.0	215.0	+157.8	0.8	+50.2	0.4	+1.09	-0.37	60.9	1.0	-	-	-	-	-	-	-
#526	219.0	221.0	222.0	+162.0	2.8	+68.2	1.6	+1.21	-0.38	49.1	0.8	-	-	-	-	-	-	-
#529	248.0	257.0	274.0	+132.3	2.6	+2.5	1.3	+0.93	-0.27	62.4	1.9	-	-	-	-	-	-	-
#530	296.0	302.0	309.0	+192.1	1.0	-18.1	1.6	+0.95	-0.39	68.1	0.7	-	-	-	-	-	-	-
#533	100.0	119.0	129.0	+41.5	2.0	+10.7	0.8	+0.97	+0.30	68.9	0.7	-	-	-	-	-	-	-
#549	104.0	112.0	141.0	+20.5	2.9	+46.6	2.6	+1.07	+0.37	60.2	1.9	-	-	-	-	-	-	-
#569	306.0	312.0	319.0	+179.2	2.5	-34.9	2.1	+0.92	-0.40	58.2	1.7	-	-	-	-	-	-	-

Table 8: Catalog of sporadic background sources. The first column contains the ID assigned to sporadic source in MeGun methodology, while in the second column there is the name tag used to identify it. Then, following column contains the extended name of the source. The fourth and fifth columns present the reference radiant ecliptic longitude λ and the associated width. Next, the sixth and seventh columns contain values of the reference radiant ecliptic latitude β and the associated width. The next columns is reserved for the average geocentric velocity computed from the distribution in [45]. The last three columns contain sporadic source relative strengths. The strengths scaled to include the ST source (assumed symmetric to the NT one) are listed in column nine. The original corrected relative strengths reported in [45] are found in column ten. The relative strengths from [30] including also the ISO source are listed in column eleven. Radiant direction is not defined for ISO. Data and velocity distribution from [45].

#ID	**Tag**	**Source**	λ [deg]		β [deg]		V [km s^{-1}]	S [−]		
			μ_λ	σ_λ	μ_β	σ_β	μ_V	-	[45]	[30]
#0	ISO	Isotropic	-	-	-	-	-	-	-	0.42
#-1	HE	Helion	+342	15	+0.2	10	27.0	0.28	0.31	0.20
#-2	AH	Anti Helion	+196	15	+0.2	10	26.3	0.34	0.37	0.20
#-3	NT	North Toroidal	+275	13	+56	9	30.8	0.10	0.11	0.05
#-4	ST	South Toroidal	+275	13	-56	9	30.8	0.10	0.11	0.05
#-5	NA	North Apex	+270	21	+18	12	43.8	0.09	0.10	0.04
#-6	SA	South Apex	+260	19	-32	12	43.1	0.09	-	0.04

Table 9: Summary of observational data about HR($\lambda_\odot$) and population index $\chi(\lambda_\odot)$ for sporadic background. Data taken from [50].

$\approx \lambda_\odot$ [deg]	HR [h^{-1}]		χ [−]
	μ_{HR}	σ_{HR}	
0	7.7	1.1	2.95
120	10.9	1.8	2.82
180	11.6	1.4	2.94
290	9.1	1.6	3.06

B Scaling from Earth to Moon

The phenomena to take into account when scaling are: gravitational acceleration, gravitational focusing, meteoroid filament density, and the correction for the different target area between Earth and Moon [1, 6, 39]. The procedure can be summarized in six steps: i) accounting for the Earth's gravitational acceleration $f_{\mathrm{acc},\oplus} = 1 + \frac{2\mu_\oplus}{R_\oplus V^2}$ and focusing $f_{\mathrm{foc},\oplus} = 1 + \frac{2\mu_\oplus}{R_\oplus V^2}$, where V is the geocentric velocity; ii) correcting for the smaller Moon's target area by means of the equatorial radii ratio $f_A = \frac{R_☾^2}{R_\oplus^2}$; iii) adding Earth's gravitational acceleration at Moon's distance [1] as $f_{\mathrm{acc},\oplus@☾} = 1 + \frac{2\mu_\oplus}{d_{\oplus☾}\, V^2}$; iv) accounting for the Moon's gravitational acceleration $f_{\mathrm{acc},☾} = 1 + \frac{2\mu_☾}{R_☾\, V^2}$ and focusing $f_{\mathrm{acc},☾} = 1 + \frac{2\mu_☾}{R_☾\, V^2}$; v) neglecting the meteoroid filament density variation assuming $f_{\mathrm{fil}} = 1$ as in [6, 39]; vi) finally, coefficients f_1 and f_2 are computed as follows $f_1 = f_{\mathrm{fil}}\, f_A\, \frac{f_{\mathrm{foc},☾}}{f_{\mathrm{foc},\oplus}}$ and $f_2 = \frac{f_{\mathrm{acc},\oplus}}{f_{\mathrm{acc},☾}\ f_{\mathrm{acc},\oplus@☾}}$.

C Proof that a meteoroid flux power law is a cumulative distribution of a Pareto distribution

The minimum impact kinetic energy $\mathrm{KE}_{\mathrm{min}}$ and s do not depend on time, they can be moved out of integral in Equation (1). The same is valid for Equation (7). Thus, a form of this type can be derived in general

$$\mathcal{N}_{\mathrm{KE}} = \mathcal{K}\,(\mathrm{KE})^{1-s} \tag{24}$$

where $\mathcal{K}$ is a constant. $\mathcal{N}$ is the cumulative number of impacts with kinetic energy greater than KE. Hence, the cumulative distribution function $P(\mathrm{KE})$ (previous fixing a minimum kinetic energy $\mathrm{KE}_{\mathrm{min}}$) can be written for $\mathrm{KE} \geq \mathrm{KE}_{\mathrm{min}}$ as

$$P(\mathrm{KE}) = \int_{\mathrm{KE}_{\mathrm{min}}}^{\mathrm{KE}} p(x)\mathrm{d}x = \frac{\mathcal{N}_{\mathrm{KE}_{\mathrm{min}}} - \mathcal{N}_{\mathrm{KE}}}{\mathcal{N}_{\mathrm{KE}_{\mathrm{min}}}} = 1 - \left(\frac{\mathrm{KE}}{\mathrm{KE}_{\mathrm{min}}}\right)^{1-s} \tag{25}$$

where $p(x)$ is the probability density function of the random variable KE. Deriving with respect to KE, the expression of the probability density function is obtained

$$\frac{\mathrm{d}P(\mathrm{KE})}{\mathrm{dKE}} = p(\mathrm{KE}) = (s-1)\,\frac{(\mathrm{KE}_{\mathrm{min}})^{s-1}}{(\mathrm{KE})^s} \tag{26}$$

which is the probability density function of a Pareto distribution with $\alpha = (s-1)$. s is computed through Equation (2) using the population index value χ.

[1] The assumed Earth–Moon distance $d_{\oplus☾}$ is the time-averaged distance between Earth and Moon centers according to [59].

References

[1] J. Oberst, A. Christou, et al. "The present-day flux of large meteoroids on the lunar surface–A synthesis of models and observational techniques". In: *Planetary and Space Science* 74.1 (2012), pp. 179–193. DOI: 10.1016/j.pss.2012.10.005.

[2] E. J. Speyerer, R. Z. Povilaitis, et al. "Quantifying crater production and regolith overturn on the Moon with temporal imaging". In: *Nature* 538.7624 (2016), pp. 215–218. DOI: 10.1038/nature19829.

[3] D. Koschny and J. Borovicka. "Definitions of terms in meteor astronomy". In: *WGN, Journal of the International Meteor Organization* 45.5 (2017), pp. 91–92.

[4] D. Koschny, R. H. Soja, et al. "Interplanetary dust, meteoroids, meteors and meteorites". In: *Space science reviews* 215.4 (2019), pp. 1–62. DOI: 10.1007/s11214-019-0597-7.

[5] R. M. Suggs, D. E. Moser, et al. "The flux of kilogram-sized meteoroids from lunar impact monitoring". In: *Icarus* 238.Supplement C (2014), pp. 23–36. DOI: 10.1016/j.icarus.2014.04.032.

[6] J. M. Madiedo, J. L. Ortiz, et al. "Analysis of Moon impact flashes detected during the 2012 and 2013 Perseids". In: *Astronomy & Astrophysics* 577.May (2015), A118. DOI: 10.1051/0004-6361/201525656.

[7] P. Brown, R. E. Spalding, et al. "The flux of small near-Earth objects colliding with the Earth." In: *Nature* 420.6913 (2002), pp. 294–296. DOI: 10.1038/nature01238.

[8] O. P. Popova, P. Jenniskens, et al. "Chelyabinsk airburst, damage assessment, meteorite recovery, and characterization". In: *Science* 342.6162 (2013), pp. 1069–1073. DOI: 10.1126/science.1242642.

[9] C. Avdellidou, E. Munaibari, et al. "Impacts on the Moon: Analysis methods and size distribution of impactors". In: *Planetary and Space Science* 200 (2021), p. 105201. DOI: 10.1016/j.pss.2021.105201.

[10] A. Liakos, A. Z. Bonanos, et al. "NELIOTA: Methods, statistics, and results for meteoroids impacting the Moon". In: *Astronomy & Astrophysics* 633 (2020), A112. DOI: 10.1051/0004-6361/201936709.

[11] M. Yanagisawa, Y. Uchida, et al. "Low dispersion spectra of lunar impact flashes in 2018 Geminids". In: *Planetary and Space Science* 195 (2021), p. 105131. DOI: 10.1016/j.pss.2020.105131.

[12] P. Jenniskens, Q. Nénon, et al. "CAMS confirmation of previously reported meteor showers". In: *Icarus* 266 (2016), pp. 355–370. DOI: 10.1016/j.icarus.2015.08.014.

[13] P. Jenniskens, Q. Nénon, et al. “CAMS newly detected meteor showers and the sporadic background”. In: *Icarus* 266 (2016), pp. 384–409. DOI: 10.1016/j.icarus.2015.11.009.

[14] P. Jenniskens, Q. Nénon, et al. “The established meteor showers as observed by CAMS”. In: *Icarus* 266 (2016), pp. 331–354. DOI: 10.1016/j.icarus.2015.09.013.

[15] J. L. Ortiz, F. J. Aceituno, et al. “Detection of sporadic impact flashes on the Moon: Implications for the luminous efficiency of hypervelocity impacts and derived terrestrial impact rates”. In: *Icarus* 184.2 (2006), pp. 319–326. DOI: 10.1016/j.icarus.2006.05.002.

[16] J. L. Ortiz, J. M. Madiedo, et al. “Lunar impact flashes from geminids: Analysis of luminous efficiencies and the flux of large meteoroids on earth”. In: *Monthly Notices of the Royal Astronomical Society* 454.1 (2015), pp. 344–352. DOI: 10.1093/mnras/stv1921.

[17] R. Walker, D. Binns, et al. “Deep-space CubeSats: thinking inside the box”. In: *Astronomy & Geophysics* 59.5 (2018), pp. 5–24. DOI: 10.1093/astrogeo/aty232.

[18] F. Topputo, G. Merisio, et al. “Current Status of LUMIO Mission: Characterizing Lunar Meteoroid Impacts with a CubeSat”. In: *72nd International Astronautical Congress (IAC 2021)*. 2021.

[19] G. Merisio, C. Giordano, et al. “Predicting the Scientific Outcome of the LUMIO Lunar Cubesat”. In: *71st International Astronautical Congress (IAC 2020)*. 2020.

[20] A. M. Cipriano, D. A. Dei Tos, et al. “Orbit design for LUMIO: The lunar meteoroid impacts observer”. In: *Frontiers in Astronomy and Space Sciences* 5 (2018), p. 29. DOI: 10.3389/fspas.2018.00029.

[21] A. Cervone, F. Topputo, et al. “LUMIO: A CubeSat for observing and characterizing micro-meteoroid impacts on the Lunar far side”. In: *Acta Astronautica* 195 (2022), pp. 309–317. DOI: 10.1016/j.actaastro.2022.03.032.

[22] A. Cervone, S. Speretta, et al. “Selection of the Propulsion System for the LUMIO Mission: an Intricate Trade-Off Between Cost, Reliability and Performance”. In: *72nd International Astronautical Congress (IAC 2021)*. 2021.

[23] A. Cervone, F. Topputo, et al. “Design Challenges and Opportunities Offered by the LUMIO Spacecraft: a CubeSat for Observing and Characterizing Micro-Meteoroid Impacts on the Lunar Far Side”. In: *72nd International Astronautical Congress (IAC 2021)*. 2021.

[24] A. Cervone, F. Topputo, et al. “Phase A Design of the LUMIO Spacecraft: a CubeSat for Observing and Characterizing Micro-Meteoroid Impacts on the Lunar Far Side”. In: *71st International Astronautical Congress (IAC 2020)*. 2020.

[25] P. B. Babadzhanov and G. I. Kokhirova. "Densities and porosities of meteoroids". In: *Astronomy & Astrophysics* 495.1 (2009), pp. 353–358. DOI: 10.1051/0004-6361:200810460.

[26] P. Brown, R. J. Weryk, et al. "A meteoroid stream survey using the Canadian Meteor Orbit Radar: I. Methodology and radiant catalogue". In: *Icarus* 195.1 (2008), pp. 317–339. DOI: 10.1016/j.icarus.2007.12.002.

[27] P. Brown, D. K. Wong, et al. "A meteoroid stream survey using the Canadian Meteor Orbit Radar: II: Identification of minor showers using a 3D wavelet transform". In: *Icarus* 207.1 (2010), pp. 66–81. DOI: 10.1016/j.icarus.2009.11.015.

[28] P. Jenniskens. "Meteor stream activity I. The annual streams". In: *Astronomy & Astrophysics* 287 (1994), pp. 990–1013.

[29] P. Jenniskens and P. M. M. Jenniskens. *Meteor showers and their parent comets*. Cambridge University Press, 2006, pp. 585–766.

[30] A. Taylor and N. McBride. "A radiant-resolved meteoroid model". In: *Second European Conference on Space Debris*. Vol. 393. 1997, p. 375.

[31] D. Koschny and J. McAuliffe. "Estimating the number of impact flashes visible on the Moon from an orbiting camera". In: *Meteoritics and Planetary Science* 44.12 (2009), pp. 1871–1875. DOI: 10.1111/j.1945-5100.2009.tb01996.x.

[32] L. R. Bellot Rubio, J. L. Ortiz, et al. "Observation and Interpretation of Meteoroid Impact Flashes on the Moon". In: *Earth, Moon, and Planets* 82.0 (Jan. 1998), pp. 575–598. DOI: 10.1023/A:1017097724416.

[33] D. E. Moser, R. M. Suggs, et al. "Luminous efficiency of hypervelocity meteoroid impacts on the moon derived from the 2006 Geminids, 2007 Lyrids, and 2008 Taurids". In: *Meteoroids: The Smallest Solar System Bodies* 1 (2011), p. 142.

[34] P. Jenniskens, P. S. Gural, et al. "CAMS: Cameras for Allsky Meteor Surveillance to establish minor meteor showers". In: *Icarus* 216.1 (2011), pp. 40–61. DOI: 10.1016/j.icarus.2011.08.012.

[35] R. Fuse, S. Abe, et al. "An experimental study of the impact flash: The relationship between luminous efficiency and vacuum level". In: *Planetary and Space Science* 187 (2020), p. 104921. DOI: 10.1016/j.pss.2020.104921.

[36] W. R. Swift, D. E. Moser, et al. "An Exponential Luminous Efficiency Model for Hypervelocity Impact into Regolith". In: *Proceedings of the Meteoroids 2010 Conference*. 2011, pp. 125–141.

[37] D. E. Gault. "Impact cratering". In: *A primer in lunar geology*. 1974.

[38] H. J. Melosh. *Impact cratering: A geologic process*. Oxford University Press, New York, 1989, pp. 1–245.

[39] J. M. Madiedo, J. L. Ortiz, et al. "MIDAS: Software for the detection and analysis of lunar impact flashes". In: *Planetary and Space Science* 111 (2015), pp. 105–115. DOI: 10.1016/j.pss.2015.03.018.

[40] C. H. Acton. “Ancillary data services of NASA’s navigation and ancillary information facility”. In: *Planetary and Space Science* 44.1 (1996), pp. 65–70. DOI: 10.1016/0032-0633(95)00107-7.

[41] C. H. Acton, N. Bachman, et al. “A look towards the future in the handling of space science mission geometry”. In: *Planetary and Space Science* 150 (2018), pp. 9–12. DOI: 10.1016/j.pss.2017.02.013.

[42] T. J. Jopek and Z. Kaňuchová. “IAU Meteor Data Center—the shower database: a status report”. In: *Planetary and Space Science* 143 (2017), pp. 3–6. DOI: 10.1016/j.pss.2016.11.003.

[43] P. Jenniskens, T. J. Jopek, et al. “On how to report new meteor showers”. In: *Ongoing meteor work* (2009), p. 19.

[44] M. D. Campbell-Brown. “Directional variation of sporadic meteor activity and velocity”. In: *Earth, Moon, and Planets* 102.1 (2008), pp. 79–84. DOI: 10.1007/s11038-007-9152-8.

[45] M. D. Campbell-Brown. “High resolution radiant distribution and orbits of sporadic radar meteoroids”. In: *Icarus* 196.1 (2008), pp. 144–163. DOI: 10.1016/j.icarus.2008.02.022.

[46] J. L. Chau, R. F. Woodman, et al. “Sporadic meteor sources as observed by the Jicamarca high-power large-aperture VHF radar”. In: *Icarus* 188.1 (2007), pp. 162–174. DOI: 10.1016/j.icarus.2006.11.006.

[47] D. Janches, S. Close, et al. “The Southern Argentina Agile MEteor Radar Orbital System (SAAMER-OS): an initial sporadic meteoroid orbital survey in the southern sky”. In: *The Astrophysical Journal* 809.1 (2015), pp. 36, 1–16. DOI: 10.1088/0004-637X/809/1/36.

[48] *Space engineering. Space environment.* Tech. rep. ECSS-E-ST-10-04C Rev.1, 15 June 2020. 2020.

[49] A. V. Moorhead, A. Kingery, et al. “NASA’s Meteoroid engineering model 3 and its ability to replicate spacecraft impact rates”. In: *Journal of Spacecraft and Rockets* 57.1 (2020), pp. 160–176. DOI: 10.2514/1.A34561.

[50] A. Dubietis and R. Arlt. “Periodic variability of visual sporadic meteor rates”. In: *Earth, Moon, and Planets* 106.2-4 (2010), pp. 105–111. DOI: 10.1007/s11038-010-9351-6.

[51] L. R. Bellot Rubio, J. L. Ortiz, et al. “Luminous Efficiency in Hypervelocity Impacts from the 1999 Lunar Leonids”. In: *The Astrophysical Journal Letters* 542.1 (2000), pp. L65–L68. DOI: 10.1086/312914.

[52] D. W. R. McKinley. *Meteor science and engineering.* New York, McGraw-Hill, 1961, pp. 104–144.

[53] D. W. Hughes. “P/Halley dust characteristics-A comparison between Orionid and Eta Aquarid meteor observations and those from the flyby spacecraft”. In: *Astronomy & Astrophysics* 187 (1987), pp. 879–888. DOI: 10.1007/978-3-642-82971-0_149.

[54] M. Kresáková. "The magnitude distribution of meteors in meteor streams". In: *Contributions of the Astronomical Observatory Skalnate Pleso* 3 (1966).

[55] A. Z. Bonanos, C. Avdellidou, et al. "NELIOTA: First temperature measurement of lunar impact flashes". In: *Astronomy & Astrophysics* 612 (2018), A76. DOI: 10.1051/0004-6361/201732109.

[56] S. Bouley, D. Baratoux, et al. "Power and duration of impact flashes on the Moon: Implication for the cause of radiation". In: *Icarus* 218.1 (2012), pp. 115–124. DOI: 10.1016/j.icarus.2011.11.028.

[57] K. A. Holsapple. "The scaling of impact processes in planetary sciences". In: *Annual Review of Earth and Planetary Sciences* 21.1 (1993), pp. 333–373.

[58] M. S. Bessell. "UBVRI photometry II: The cousins VRI System, its temperature and absolute flux calibration, and relevance for two-dimensional photometry." In: *Publications of the Astronomical Society of the Pacific* 91.543 (1979), p. 589. DOI: 10.1086/130542.

[59] T. W. Murphy. "Lunar laser ranging: the millimeter challenge". In: *Reports on Progress in Physics* 76.7 (2013), p. 076901. DOI: 10.1088/0034-4885/76/7/076901.

[60] R. M. Suggs, S. R. Ehlert, et al. "A comparison of radiometric calibration techniques for lunar impact flashes". In: *Planetary and Space Science* 143 (2017), pp. 225–229. DOI: 10.1016/j.pss.2017.04.016.

[61] M. D. Campbell-Brown and J. Jones. "Annual variation of sporadic radar meteor rates". In: *Monthly Notices of the Royal Astronomical Society* 367.2 (2006), pp. 709–716. DOI: 10.1111/j.1365-2966.2005.09974.x.

[62] Z. Ceplecha, J. Borovička, et al. "Meteor Phenomena and Bodies". In: *Space Science Review* 84.3 (1998), pp. 327–471. DOI: 10.1023/A:1005069928850.

[63] C. Avdellidou and J. Vaubaillon. "Temperatures of lunar impact flashes: mass and size distribution of small impactors hitting the Moon". In: *Monthly Notices of the Royal Astronomical Society* 484.4 (2019), pp. 5212–5222. DOI: 10.1093/mnras/stz355.